electronics

MDPI

Article

IPCB: Intelligent Pseudolite Constellation Based on High-Altitude Balloons

Yi Qu [1,2,*], Sheng Wang [1,2], Tianshi Pan [1] and Hui Feng [1]

[1] Aerospace Information Research Institute, Chinese Academy of Sciences, Beijing 100094, China
[2] University of Chinese Academy of Sciences, Beijing 100049, China
* Correspondence: quyi@aircas.ac.cn

Abstract: IPCBs (Intelligent Pseudolite Constellations based on high-altitude balloons) are a novel type of air-based pseudolite application with many advantages. Compared with ground-based pseudolites and traditional air-based pseudolites, IPCBs have a wider coverage and a lower energy requirement. Compared with LEO satellite constellations, IPCBs have a stronger signal, a lower cost, and a shorter deployment period. These merits give promising potential to IPCBs. In IPCB applications, one of the key factors is geometry configuration, which is deeply influenced by the balloon's unique features. The basic idea of this paper is to pursue a strategy to improve IPCB geometry performance by using diverse winds at different altitudes and balloons' capability of altering flight altitude intelligently. Starting with a brief introduction to IPCBs, this paper defines an indicator to assess IPCB geometry performance, an approach to adjust IPCB geometry configuration and an IPCB geometry configuration planning algorithm. Next, a series of simulations are implemented with an IPCB composed of six pseudolites in winds with/without a quasi-zero wind layer. Some IPCB geometry configurations are analyzed, and their geometry performances are compared. Simulation results show the effectiveness of the proposed algorithm and the influence of the quasi-zero wind layer on IPCB performance.

Keywords: intelligent pseudolite; constellation; high altitude balloon

Citation: Qu, Y.; Wang, S.; Pan, T.; Feng, H. IPCB: Intelligent Pseudolite Constellation Based on High-Altitude Balloons. *Electronics* **2024**, *13*, 2095. https://doi.org/10.3390/electronics13112095

Academic Editor: Silvia Liberata Ullo

Received: 12 April 2024
Revised: 5 May 2024
Accepted: 13 May 2024
Published: 28 May 2024

1. Introduction

Pseudolites are transmitters that can emit navigation signals to improve GNSS performance or to provide navigation service independently [1–7]. An intelligent pseudolite based on high-altitude balloons (IPBs) is a type of novel air-based pseudolite that utilizes a high-altitude balloon as a platform. An intelligent pseudolite constellation based on high-altitude balloons (IPCBs) is composed of multiple IPBs, which can provide emergency positioning service and regional positioning service independently.

As an excellent solution for regional positioning, ICPBs have many advantages. Compared with ground-based pseudolites and traditional air-based pseudolites, IPCBs have a wider coverage and can serve more users because their flight altitude can reach tens of kilometers [8,9]. Furthermore, IPCBs have a low energy requirement since they can accomplish its flight primarily relying on buoyancy and wind rather than oil or electricity [10,11]. Compared with LEO satellite constellations, IPCBs have a stronger signal, a lower cost, and a shorter deployment period [12,13]. In addition, the continuous residence duration of an IPB over a service area is longer than that of an LEO satellite, which can reduce navigation signal lock-lose and cycle slip caused by satellite switching [14–16]. Also, the IPCB operation and maintenance burden is less than that of an LEO satellite constellation because an LEO satellite constellation usually comprises a large number of satellites [17,18]. These merits give promising potential to IPCB applications.

In the application of IPCBs, geometry configuration plays a critical role since it affects IPCB service performance significantly [19–22]. However, the problem becomes very

complicated because of the unique dynamic features of IPBs. Most traditional research studies about pseudolite geometry configuration are designed for static pseudowires, which are not suitable for IPCBs [23–27].

This paper centers on the problem of IPCB geometry configuration and proposes a planning algorithm that emphasizes utilizing different winds smartly. The proposed algorithm can fit the dynamic flight of IPCBs adaptively and is easy to implement. Moreover, it can achieve performance improvements by controlling IPB valves and fans only, without extra hardware cost.

The rest of this paper is organized as follows. An overview of IPCBs is described in Section 2, a performance indicator of IPCB geometry configuration is defined in Section 3, an IPCB geometry configuration adjustment approach is designed in Section 4, a series of constraints are discussed in Section 5, a planning algorithm based on whale optimization algorithm (WOA) is proposed in Section 6, simulations and discussions are presented in Section 7, and conclusions are stated in Section 8.

2. Overview of IPCB

An IPB is illustrated in Figure 1. It utilizes a high-altitude balloon as a platform, which is composed of balloon, cable, parachute, gondola, balloon controller, payloads, and other attachments, as shown in Figure 1a. The balloon controller, payloads, and other attachments are installed in the gondola. Furthermore, the balloon consists of a main helium bag and an air ballonet, which are separated by a membrane, as Figure 1b illustrates [28–30]. The main helium bag is filled with helium to provide buoyancy to the IPB, and the air ballonet is filled with air to adjust the IPB mass. Fans and valves are installed on the bottom of the balloon, which can pump air into or release air from the air ballonet. The balloon controller can perceive and adjust IPB flight status intelligently. In particular, the balloon controller can manipulate the fans and valves flexibly, enabling the IPB to adjust its mass and flight altitude in a range.

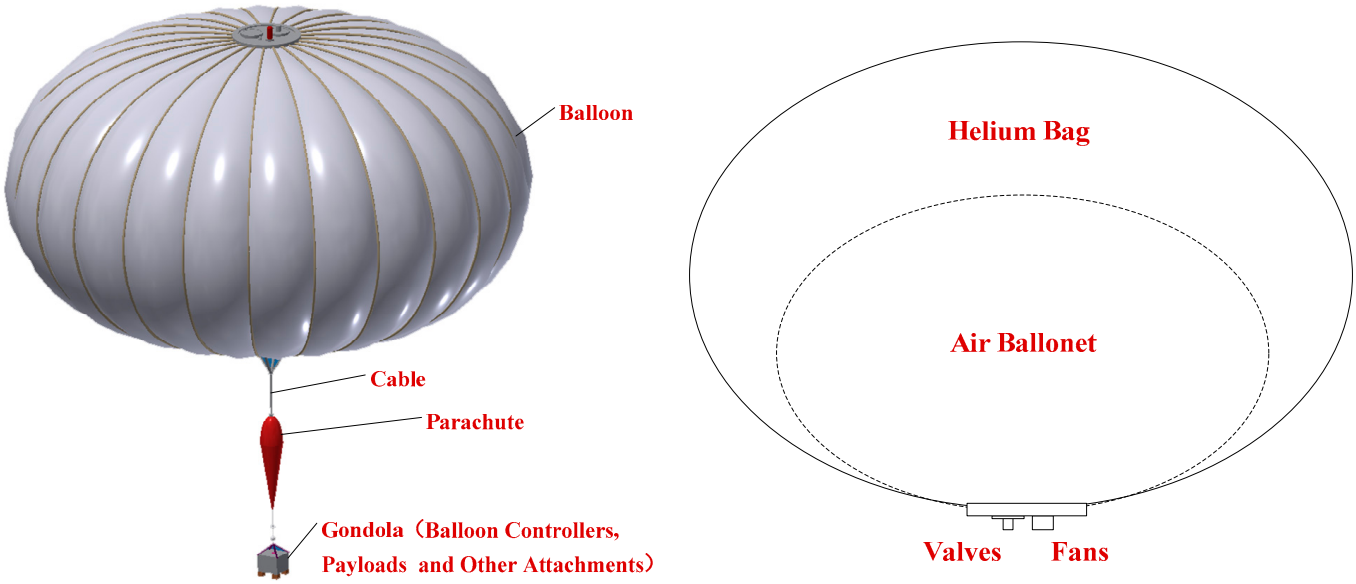

Figure 1. Structure illustration of IPB studied in this paper: (**a**) structure overview; (**b**) detailed structure of the balloon.

An IPCB is illustrated in Figure 2. It consists of multiple IPBs and can form coverage over a service area. When payloads in the IPBs normally send out navigation signals, the IPCB can provide positioning service for the area independently. During the process of

IPCB service, its geometry configuration is always changing with the wind, and the changes are highly nonlinear, which brings difficulty to IPCB geometry configuration planning.

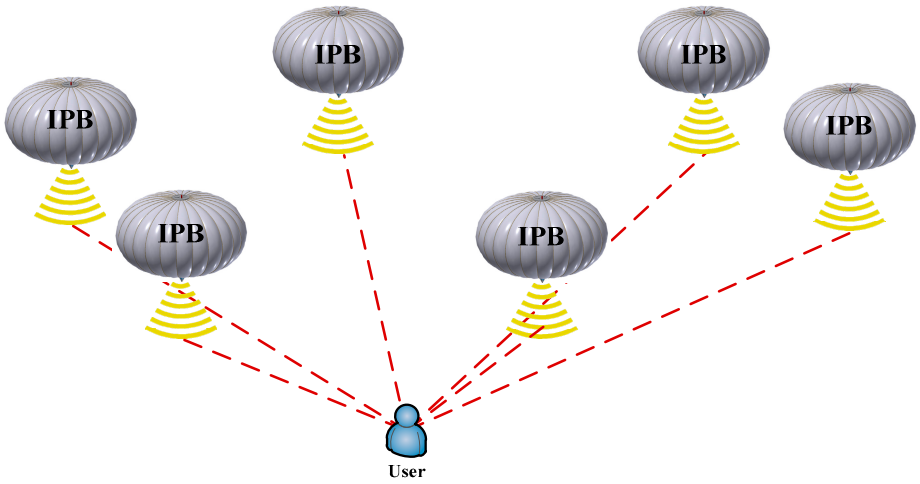

Figure 2. Illustration of IPCB in regional positioning.

3. Performance Indicator of IPCB Geometry Configuration

Assuming that an IPCB composed of n_p IPBs is deployed above the service area initially and that n_u users are selected as samples to assess IPCB geometry performance. Then, the pseudo-range equation from the j-th IPB to the i-th user at time t can be expressed by Equation (1) [31–33].

$$\rho(i,j,t) = \sqrt{(x(j,t) - x_u(i,t))^2 + (y(j,t) - y_u(i,t))^2 + (z(j,t) - z_u(i,t))^2} + ct_u(i,t) \quad (1)$$

In Equation (1), $\rho(i,j,t)$ represents the pseudo-range from the j-th IPB to the i-th user at time t; $(x(j,t), y(j,t), z(j,t))$ represents the position of the j-th IPB at time t; $(x_u(i,t), y_u(i,t), z_u(i,t))$ represents the position of the i-th user at time t; c represents the speed of light; $t_u(i,t)$ represents the clock difference of the i-th user at time t.

Equation (1) can be rewritten as Equation (2) after the first-order Taylor expansion.

$$\Delta\rho(i,j,t) = a_x(i,j,t)\Delta x_u(i,t) + a_y(i,j,t)\Delta y_u(i,t) + a_z(i,j,t)\Delta z_u(i,t) - c\Delta t_u(i,t) \quad (2)$$

In Equation (2), 'Δ' represents the difference between the Taylor expansion point and its neighborhood, $(a_x(i,j,t), a_y(i,j,t), a_z(i,j,t))$ represents the direction cosine from the i-th user to the j-th IPB at time t, which can be calculated by Equation (3).

$$\begin{aligned} a_x(i,j,t) &= \frac{x(j,t) - x_u(i,t)}{\sqrt{(x(j,t) - x_u(i,t))^2 + (y(j,t) - y_u(i,t))^2 + (z(j,t) - z_u(i,t))^2}} \\ a_y(i,j,t) &= \frac{y(j,t) - y_u(i,t)}{\sqrt{(x(j,t) - x_u(i,t))^2 + (y(j,t) - y_u(i,t))^2 + (z(j,t) - z_u(i,t))^2}} \\ a_z(i,j,t) &= \frac{z(j,t) - z_u(i,t)}{\sqrt{(x(j,t) - x_u(i,t))^2 + (y(j,t) - y_u(i,t))^2 + (z(j,t) - z_u(i,t))^2}} \end{aligned} \quad (3)$$

Equation (2) can be expanded from the j-th IPB to all the IPBs in the IPCB, which can be simplified as

$$\boldsymbol{\Delta\rho}(i,t) = \boldsymbol{H}(i,t)\boldsymbol{\Delta x}(i,t) \quad (4)$$

In Equation (4), $\boldsymbol{\Delta\rho}(i,t)$ is a vector representing pseudo-range measurement error, $\boldsymbol{\Delta x}(i,t)$ is a vector representing positioning error, and $\boldsymbol{H}(i,t)$ is an observation matrix.

Equation (4) can be rewritten as Equation (5) by the least square method.

$$\boldsymbol{\Delta x}(i,t) = (\boldsymbol{H}(i,t)^T\boldsymbol{H}(i,t))^{-1}\boldsymbol{H}(i,t)^T\boldsymbol{\Delta\rho}(i,t) \quad (5)$$

If the pseudo-range noises of different IPBs are linearly independent, with an average of 0 and a variance of σ^2, then the covariance of $\boldsymbol{\Delta x}(i,t)$ can be expressed by Equation (6) [33].

$$\mathrm{cov}(\boldsymbol{\Delta x}(i,t)) = \sigma^2(\boldsymbol{H}(i,t)^{\mathrm{T}}\boldsymbol{H}(i,t))^{-1} \tag{6}$$

From Equation (6), it can be concluded that $(\boldsymbol{H}(i,t)^{\mathrm{T}}\boldsymbol{H}(i,t))^{-1}$ reveals the magnification from a user pseudo-range measurement error to its positioning error. Given the same user pseudo-range measurement error, the smaller $(\boldsymbol{H}(i,t)^{\mathrm{T}}\boldsymbol{H}(i,t))^{-1}$ is, the smaller the positioning error is. Consequently, the square root of the trace of $(\boldsymbol{H}(i,t)^{\mathrm{T}}\boldsymbol{H}(i,t))^{-1}$ is usually treated as an important indicator to assess the influence of a constellation geometry configuration on its positioning error, named GDOP (geometric dilution of precision), which can be expressed by Equation (7) [33–36].

$$GDOP(i,t) = \sqrt{tr(\boldsymbol{H}(i,t)^{T}\boldsymbol{H}(i,t))^{-1}} \tag{7}$$

It is obvious that the value of $GDOP(i,t)$ will fluctuate due to IPCBs' dynamic movements. In particular, some IPBs in the constellation may leave approved airspace as time goes on. In such cases, they cannot continue emitting navigation signals (detailed discussion in Section 5.1), which will decrease the number of available IPBs in the constellation. Once the number of available IPBs in the constellation drops below 4, the GDOP of the IPCB is defined as infinity in this paper.

The geometry performance of an IPCB at time t can be assessed by the average GDOP of multiple users distributed in the service area, as described in Equation (8) [37].

$$GDOP(t) = \frac{1}{n_u}\sum_{i=1}^{n_u} GDOP(i,t) \tag{8}$$

It can be concluded that the objective of IPCB geometry configuration planning is to obtain the minimal $GDOP(t)$ for the whole service duration. However, this approach encounters difficulties when dealing with infinite values. To avoid such difficulties, this paper defines the performance indicator as Equation (9).

$$F = \frac{1}{n_t}\sum_{t=1}^{n_t}\frac{1}{GDOP(t)} \tag{9}$$

In Equation (9), n_t represents the expected service duration of the IPCB. The ultimate objective of IPCB geometry configuration planning is to maximize F defined in Equation (9).

4. Adjustment Approaches of IPCB Geometry Configuration

As discussed in Section 2, IPBs have little actuation capability since they are not equipped with propellers. The primary actuation they can implement is to control their valves and fans, which cannot change the IPCB geometry configuration directly. Therefore, this paper adopts an indirect adjustment approach.

In the vertical direction, IPBs can actively change their masses and flight altitudes by switching their valves and fans. Specific adjustments of each IPB can be managed by its balloon controller. In the horizontal direction, IPBs can change their trajectories with the help of local winds at different altitudes [38–40]. By combining the adjustments in the two directions, IPBs can change their flight trajectories, and the IPCB can modify its geometry configuration [9,28,41,42].

Subsequent detailed analyses will be presented based on the vertical adjustment and the horizontal adjustment of individual IPBs, respectively. The following assumptions are made to simplify the analysis.

(1) The flight altitude of an IPB is fully controllable, and its variation depends on a rise rate and a sink rate, represented by v_{rise} and v_{sink}, respectively.
(2) The horizontal velocity of an IPB is proportional to the local horizontal wind velocity.

(3) Wind velocities vary with altitude but not with horizontal location. The wind velocities and atmosphere environment are steady during IPCB service time.
(4) The influences of balloon volume variation and thermal effect on IPB motions are ignored.

4.1. Vertical Adjustment of an IPB

An IPB usually keeps its flight altitude by maintaining the balance between gravity and buoyancy, as Equation (10) shows:

$$\boldsymbol{B} = \boldsymbol{G} \tag{10}$$

In Equation (10), $\boldsymbol{B}$ represents its buoyancy, and $\boldsymbol{G}$ represents its gravity. Buoyancy $\boldsymbol{B}$ is related to the atmospheric density, volume of the balloon, and gravitation acceleration, as shown in Equation (11).

$$\boldsymbol{B} = \rho_{air}(h)V\boldsymbol{g} \tag{11}$$

In Equation (11), V represents the volume of the balloon, $\boldsymbol{g}$ represents gravitation acceleration, h represents the flight altitude of the IPB, and $\rho_{air}(h)$ represents the air density at altitude h. The air density is not a constant, and it varies in a wide range. According to the standard atmosphere model (U.S. Standard Atmosphere, 1976), its change with altitude is illustrated in Figure 3.

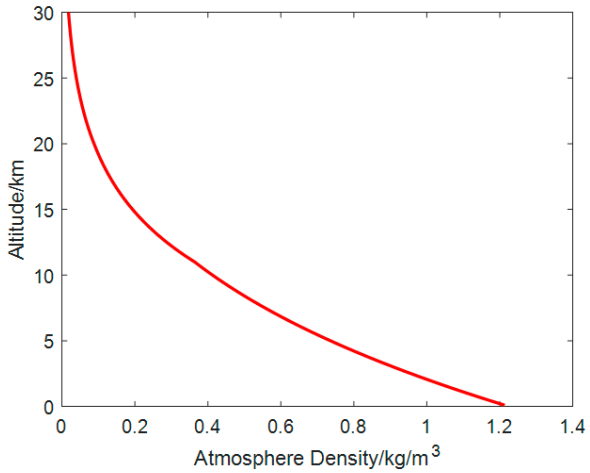

Figure 3. Atmosphere density from 0 km to 30 km.

Gravity $\boldsymbol{G}$ is related to helium mass, air mass, and the masses of others, as shown in Equation (12).

$$\boldsymbol{G} = (m_{He} + m_{air}(h) + m_{other})\boldsymbol{g} \tag{12}$$

In Equation (12), m_{He} represents the helium mass in the main helium bag, $m_{air}(h)$ represents the air mass in the air ballonet at altitude h, m_{other} represents the gross mass of balloon envelop, cable, parachute, gondola, balloon controller, payloads and other attachments.

So if a flight altitude decline is needed, an IPB can pump air into its air ballonet, which will increase its air mass $m_{air}(h)$ and gravity $\boldsymbol{G}$, making $\boldsymbol{G}$ greater than $\boldsymbol{B}$. The change in air mass can be estimated by Equation (13).

$$\Delta m = (\rho_{air}(h_s) - \rho_{air}(h_d))V \tag{13}$$

In Equation (13), h_s and h_d represent the flight altitude before adjustment and after adjustment, respectively. Due to the assumption (1) in this section, the time cost of the flight altitude adjustment Δt can be estimated by Equation (14).

$$h_s - h_d = v_{\sin k}\Delta t \tag{14}$$

In contrast, if a flight altitude ascent is needed, the IPB should release air from its air ballonet, and the time cost can be estimated by Equation (15).

$$h_s - h_d = v_{\text{rise}} \Delta t \tag{15}$$

4.2. Horizontal Adjustment of an IPB

According to assumption (2) in this section, the horizontal velocity of an IPB is proportional to the local horizontal wind velocity [38–40]. Then, the horizontal kinematics of an IPB can be described by Equation (16).

$$\begin{aligned} \dot{\lambda} &= \gamma \cdot w_z(\lambda, \phi, h, t) \\ \dot{\phi} &= \gamma \cdot w_m(\lambda, \phi, h, t) \end{aligned} \tag{16}$$

In Equation (16), λ represents the longitude of IPB position; $\dot{\lambda}$ represents the variation of λ; ϕ represents the latitude of IPB position; $\dot{\phi}$ represents the variation of ϕ; $w_z(\lambda, \phi, h, t)$ represents zonal wind velocity at position (λ, ϕ, h) and at time t; $w_m(\lambda, \phi, h, t)$ represents meridional wind velocity at position (λ, ϕ, h) and at time t; γ represents a drag coefficient of IPB in the horizontal plane.

Since it is assumed that wind velocities vary with altitude but not with horizontal location, and wind velocities are steady in IPCB service time, the relation between altitude and wind velocity is emphasized in this paper. In general, wind velocity increases as altitude increases in the troposphere, reaching a maximum of about 10~15 km. Then, wind velocity decreases, reaching a minimum in the lower portion of the stratosphere at about 18~25 km [43,44]. For simplicity, a seventh-order polynomial is employed to fit the relation between altitude and wind velocity in this paper, as described below [45–47].

$$\begin{aligned} w_m &= c_{m0} + c_{m1} h_{std} + c_{m2} {h_{std}}^2 + \cdots + c_{m7} {h_{std}}^7 \\ w_z &= c_{z0} + c_{z1} h_{std} + c_{z2} {h_{std}}^2 + \cdots + c_{z7} {h_{std}}^7 \end{aligned} \tag{17}$$

In Equation (17), $\boldsymbol{c_m}$ and $\boldsymbol{c_z}$ represent meridional wind coefficients and zonal wind coefficients, respectively. h_{std} represents normalized altitude, which can be calculated by Equation (18).

$$h_{std} = (h - \mu_d)/\sigma_d \tag{18}$$

In Equation (18), μ_d and σ_d are both normalized parameters. Figure 4 illustrates wind fittings for a specific area in March, June, September, and December.

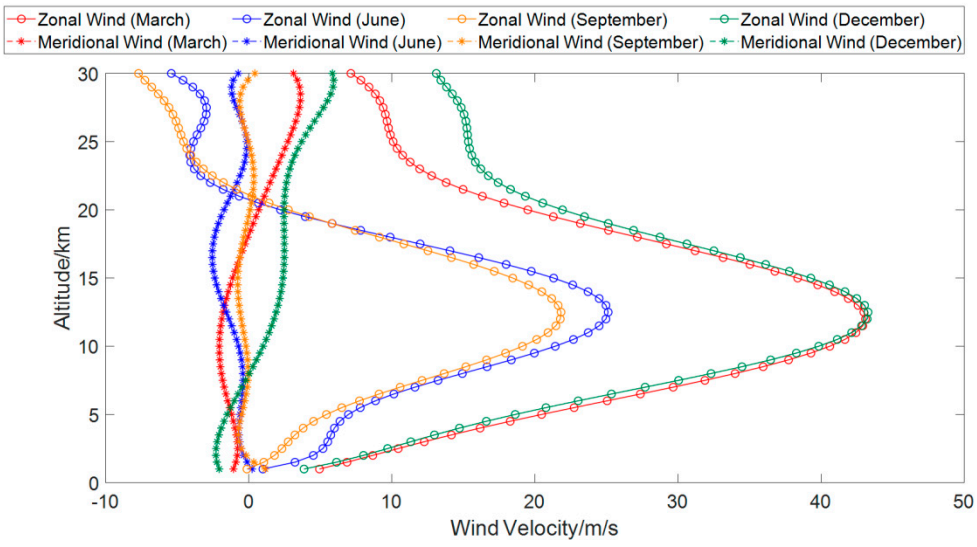

Figure 4. Wind fittings from 1 km to 30 km for a specific region.

From Figure 4, it can be seen that wind velocity changes remarkably with altitude, which provides opportunities for IPBs to adjust their horizontal trajectories utilizing different winds. In particular, a so-called "quasi-zero wind layer" existed at an altitude of about 21 km in June and September, as shown in Figure 4. At altitudes up and down the quasi-zero wind layer, the direction of zonal wind reverses, and the magnitude of meridional wind is small, which is beneficial to IPBs to lengthen their flight time in specific airspace [48–53].

5. Constraints of IPCB Geometry Configuration

IPCB geometry configuration faces many constraints because of its unique features and management strategy, such as airspace constraints, flight altitude constraints, and time interval constraints.

5.1. Airspace Constraint

Airspace is the space in which an IPCB is approved to fly at a certain time. Within the approved airspace, an IPB can fly with its gondola, and its payloads, such as signal generators and transmitters, can run normally. Once an IPB flies out of the approved airspace, its gondola will be cut off from its balloon, and the payloads in the gondola will be switched off, making it impossible for the IPB to emit navigation signals. So, the longitudes and latitudes of each IPB in the IPCB should vary depending on the extent of the approved airspace.

5.2. Flight Altitude Constraint

As discussed above, the flight altitude adjustment of an IPB is achieved by changing its air ballonet volume, which cannot change infinitely. The air ballonet volume of an IPB can only vary in a feasible range, and so does its flight altitude. During IPCB geometry configuration planning, the flight altitudes of all the IPBs should not go beyond the range.

5.3. Time Interval Constraint

Due to the low-density atmosphere at IPCB flight altitudes and the limited capacity of fans, IPCB geometry configuration adjustment requires a long time. So, the time interval between adjacent adjustment actuations should be greater than the maximum trajectory adjustment time required by all the IPBs in the constellation. In this paper, Equations (14) and (15) are used to estimate the time required for an IPB trajectory adjustment.

6. Planning Algorithm of IPCB Geometry Configuration

Based on the analysis above, it can be inferred that if fans and valves can be controlled properly, IPCB geometry configuration can be achieved by utilizing winds at different altitudes effectively. So, the IPCB geometry configuration planning problem can be considered a flight altitude combination problem that can be solved by heuristic algorithms.

WOA is a famous heuristic algorithm that has achieved success in many applications because of its strong robustness, effective searchability, and convenient parameter settings [54–58]. Compared with PSO (particle swarm optimization) or DE (differential evolution algorithm), WOA does not consider subjective parameter settings, such as the inertial coefficient, acceleration coefficient, and other parameters in PSO, scale factor, crossover probability, and other parameters in DE [59,60]. In addition, the performance of WOA, PSO, and DE are compared in reference [54], and WOA displays its excellent capability [54]. Therefore, this paper adopts WOA to realize IPCB geometry configuration planning.

In the planning algorithm, the flight altitudes of all the IPBs in an IPCB can be treated as a whale agent. The general procedure of the algorithm can be described as follows:

Initialize all the whale agents in the current whale population randomly (i.e., initialize the flight altitudes of all the IPBs randomly);

Acquire horizontal winds corresponding to the flight altitudes (i.e., the whale agents just initialized) by Equation (17) or from other data sources;

Calculate horizontal trajectories of all the IPBs in the IPCB by Equation (16);

Adjust the flight altitudes and horizontal trajectories of the IPCB by approaches defined in Section 4;

If the flight altitudes, horizontal trajectories, or adjusted time intervals (calculated by Equation (14) or (15)) do not meet the constraints listed in Section 5, the fitness of the whale agent is defined as 0, meaning that the corresponding IPCB geometry configuration is not feasible in the assumed conditions;

To a whale agent complying with the constraints listed in Section 5, calculate its fitness by Equation (9);

Calculate the fitness of all the whale agents and select the best whale agent in the current whale population;

Update all the whale agents in the current whale population by strategies defined in WOA, such as the "encircling prey" strategy, "bubble-net attacking" strategy, and "search for prey" strategy [54];

Implement updating iteration according to the procedure of WOA, which has been described in detail in reference [54];

When the iteration ends, an IPCB flight altitude can be obtained from the best whale agent. The flight trajectory and constellation GDOP can also be calculated from the best whale agent, forming a complete IPCB geometry configuration.

7. Simulations and Discussions

To verify the effect of the proposed algorithm, simulations are carried out in Matlab 2018b, with the context of IPCB providing independent regional positioning services.

7.1. Simulation Settings

The parameters used in the simulations are listed in Table 1.

Table 1. Parameters used in simulations.

Symbol	Physical Meaning	Value
n_p	number of IPBs in a constellation initially	6
n_t	expected service duration of an IPCB	24 h
c_m	meridional wind coefficients	−0.1338, 1.3189, −1.9669, −2.3772, 4.0187, 1.4032, −1.4290, −0.5504
c_z	zonal wind coefficients	2.1927, −7.6660, −3.0280,28.8161, −2.6879, −41.5979, 2.0248, 21.8084
λ_{min}	minimal longitude of the approved airspace	107° E
λ_{max}	maximal longitude of the approved airspace	109° E
ϕ_{min}	minimal latitude of the approved airspace	39° N
ϕ_{max}	maximal latitude of the approved airspace	41° N
h_{min}	feasible minimal flight altitude of an IPB	20 km
h_{max}	feasible maximal flight altitude of an IPB	24 km

The initial geometry configuration of the IPCB is listed in Table 2, as Figure 5a,b illustrates. Users are distributed uniformly in the service area, as Figure 5c illustrates. The average GDOP of the IPCB with initial geometry configuration is 7.47, whose distribution is illustrated in Figure 5d.

Table 2. Initial geometry configuration of the IPCB.

IPB	Longitude	Latitude	Flight Altitude
IPB 1	107.4° E	39.4° N	21 km
IPB 2	108.6° E	39.4° N	21 km
IPB 3	108.6° E	40.6° N	21 km
IPB 4	107.4° E	40.6° N	21 km
IPB 5	107.8° E	40° N	22 km
IPB 6	108.2° E	40° N	22 km

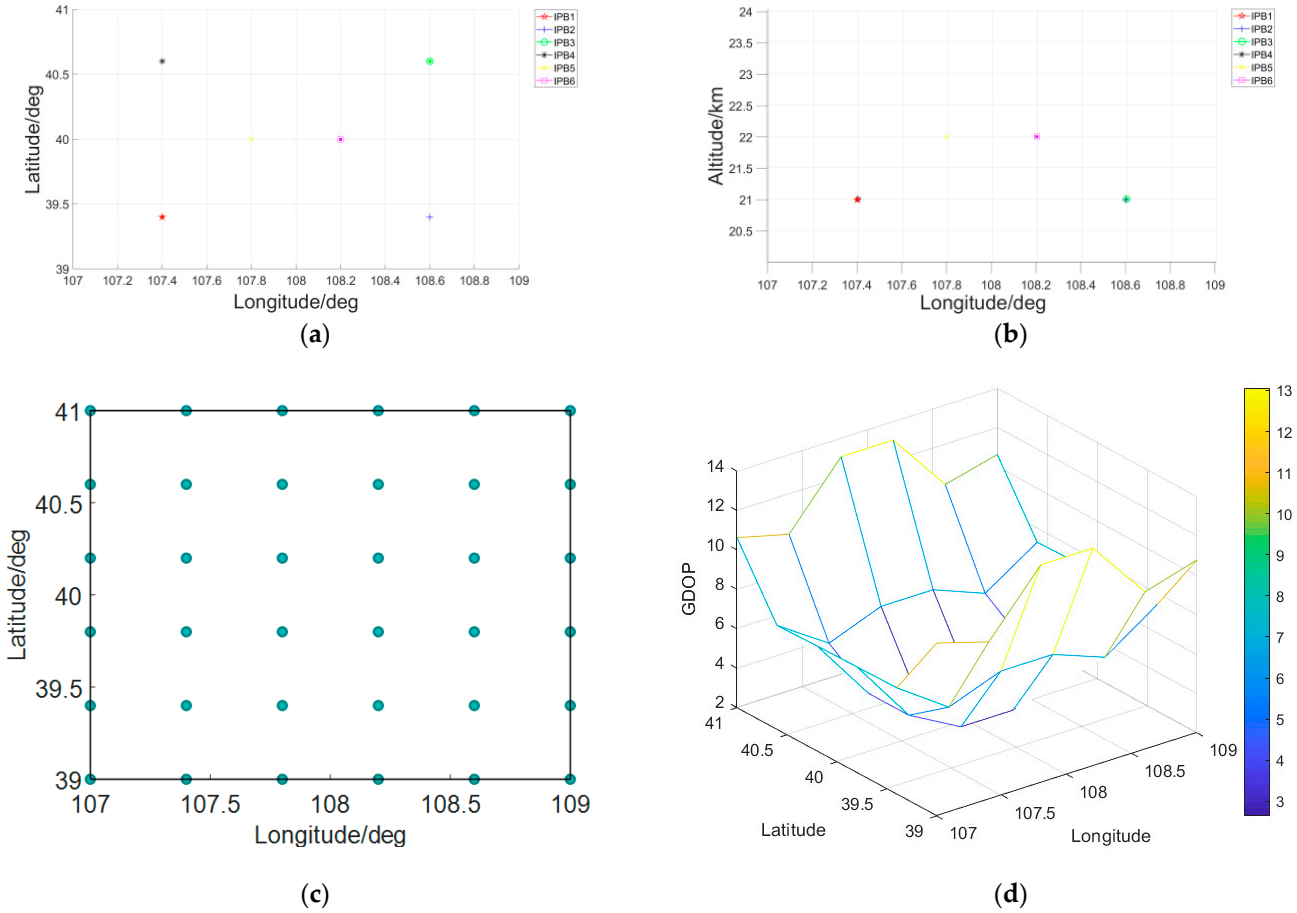

Figure 5. Initial geometry configuration, GDOP distribution of the IPCB, and user distribution: (**a**) initial horizontal layout of the IPCB; (**b**) initial flight altitude of the IPCB; (**c**) user distribution in the service area; (**d**) GDOP distribution of the IPCB with initial geometry configuration.

7.2. Simulation Result

Simulations are carried out with parameters defined in Section 7.1. Figures 6–8 illustrate the planning result. If an IPB flies out of the approved airspace, its subsequent data will not be displayed in figures.

From Figures 6–8, it can be seen that the proposed planning algorithm takes two measures to improve IPCB geometry configuration.

The first measure is to adjust IPB flight altitudes by changing their masses. It makes most IPBs in the constellation fly at an altitude of around 21 km, where wind velocity is small. This measure lengthens IPBs' flight time in the approved airspace, benefiting from keeping the number of available IPBs in the IPCB.

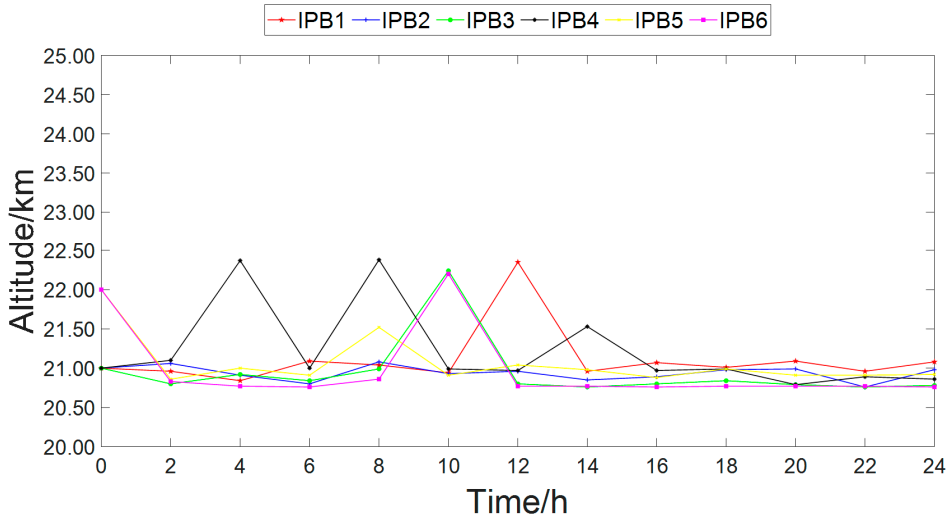

Figure 6. Flight altitude of the IPCB in its service duration.

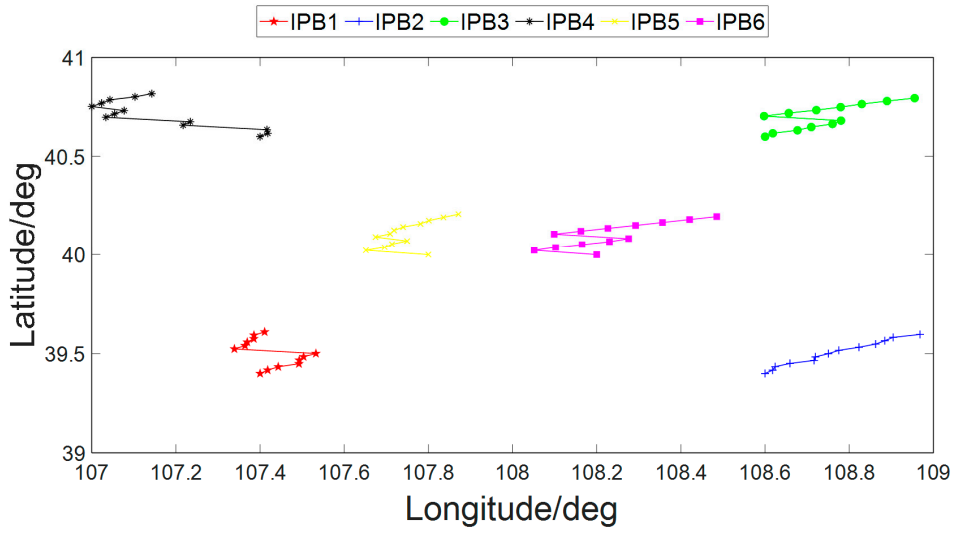

Figure 7. Horizontal trajectory of the IPCB in its service duration.

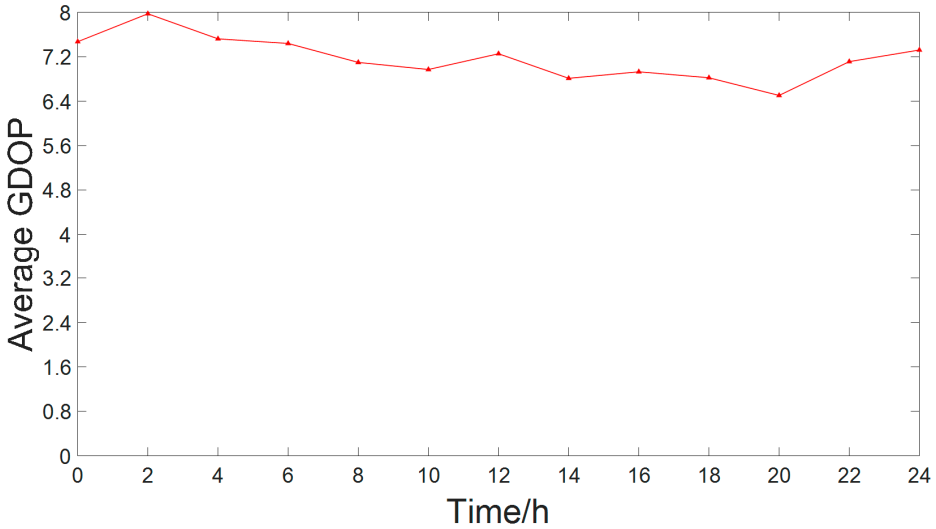

Figure 8. GDOP of the IPCB in its service duration.

The second measure is to make IPBs fly across the quasi-zero wind layer. This measure utilizes the reverse zonal wind direction to change IPBs' movement direction, which can extend IPBs' flight time in the approved airspace and adjust IPBs' horizontal trajectories, thus improving IPCB geometry configuration.

7.3. Discussion about IPCBs with Different Initial Flight Altitudes

IPBs' initial flight altitudes have a significant impact on IPCB geometry performance. In this section, the initial flight altitudes of IPB5 and IPB6 in Table 2 are modified to 20 km, 21 km, 22 km, 23 km, and 24 km, respectively, while other conditions remain untouched. The planning results of different IPCBs are listed in Figures 9–11.

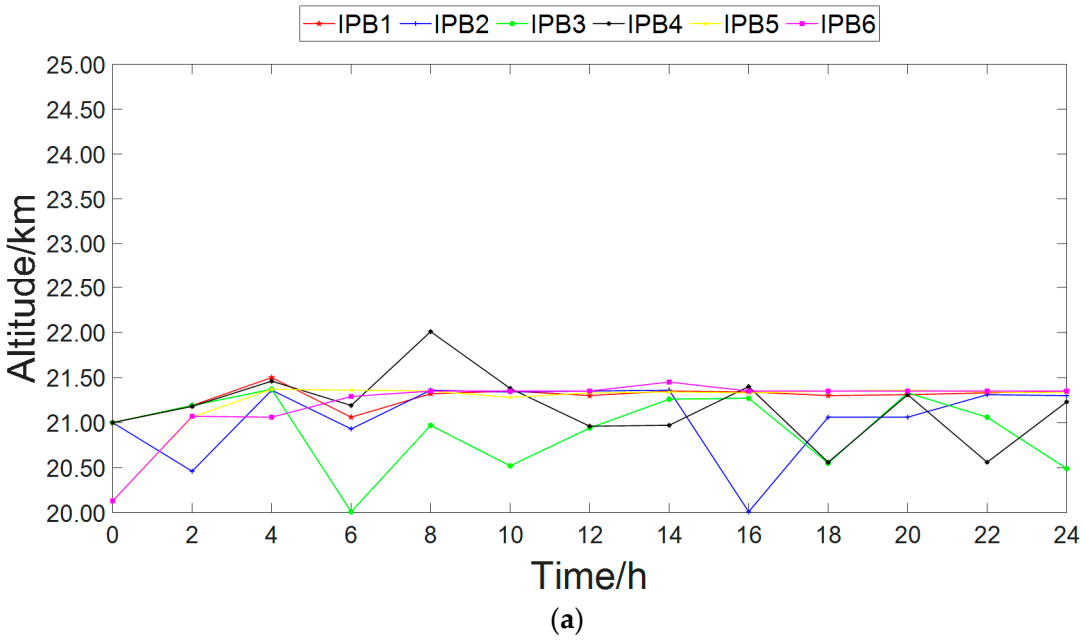

(**a**)

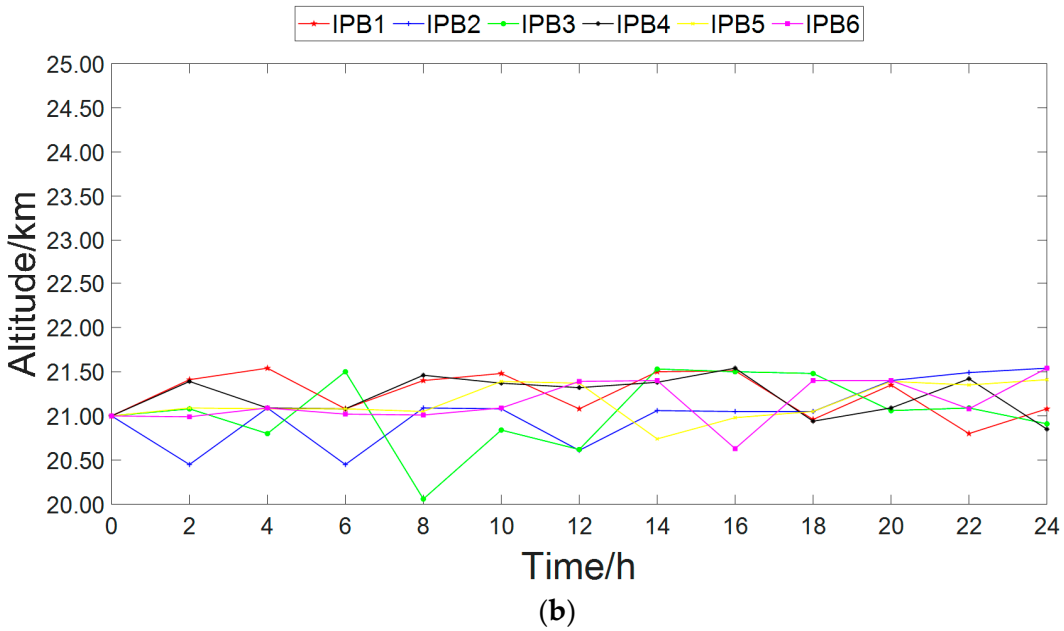

(**b**)

Figure 9. *Cont.*

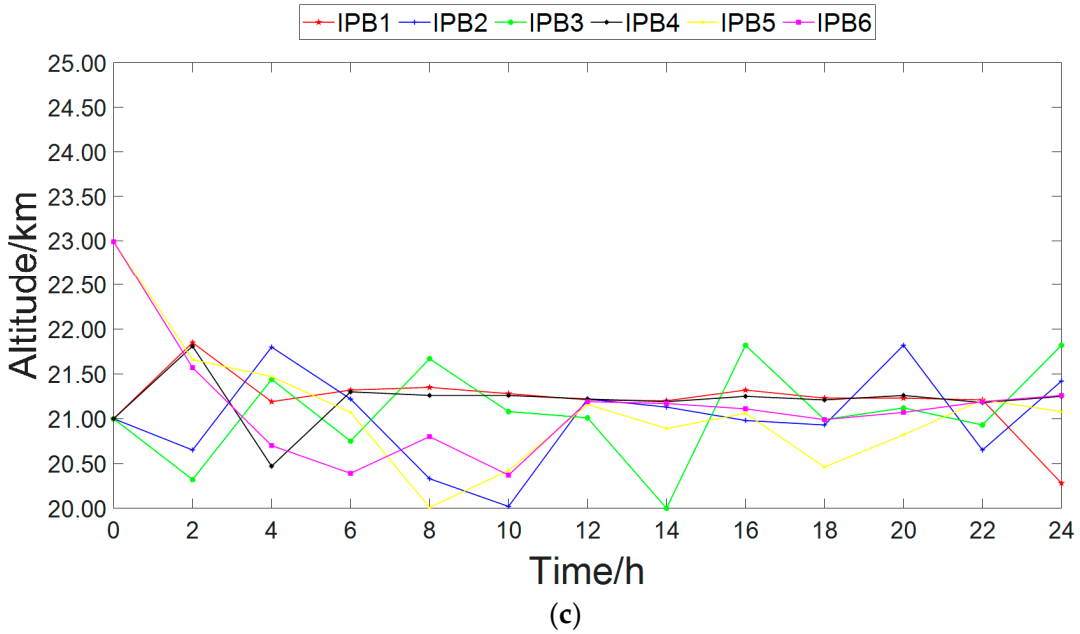

(**c**)

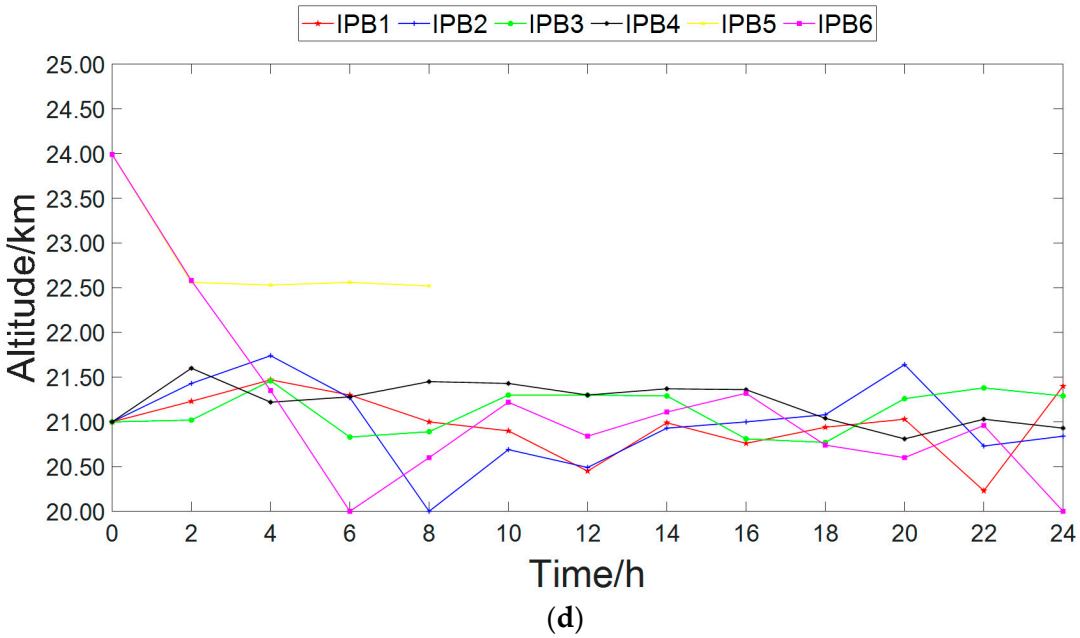

(**d**)

Figure 9. Flight altitude comparison for IPCBs with different initial flight altitudes: (**a**) IPB5 and IPB6 at 20 km initially; (**b**) IPB5 and IPB6 at 21 km initially; (**c**) IPB5 and IPB6 at 23 km initially; (**d**) IPB5 and IPB6 at 24 km initially. (Flight altitude for IPCB with IPB5 and IPB6 at 22 km initially, please refer to Figure 6).

From the comparison of Table 3, it can be seen that there are no significant performance differences in 20 km, 21 km, 22 km, and 23 km, but there is a declining tendency in 24 km. The result of 24 km can probably be attributed to the short service time of IPB5 caused by the big wind velocity. All of these are reflected in Figures 9–11.

Table 3. Simulation results for IPCBs with different initial flight altitudes.

Initial Flight Altitude of IPB5 and IPB6/km	Average GDOP
20	7.26
21	7.14
22	7.32
23	7.47
24	8.64

In addition, from Figure 11, it can be seen that for the listed initial flight altitudes, the higher the initial flight altitude is, the better the initial GDOP is. However, the IPCB with the highest initial flight altitude has the fastest performance deterioration due to the big wind velocity at the highest altitude. Therefore, if short-term performance is pursued, higher initial flight altitudes may be preferred over lower altitudes. If long-term performance is pursued, initial flight altitudes near the quasi-zero wind layer may be preferred.

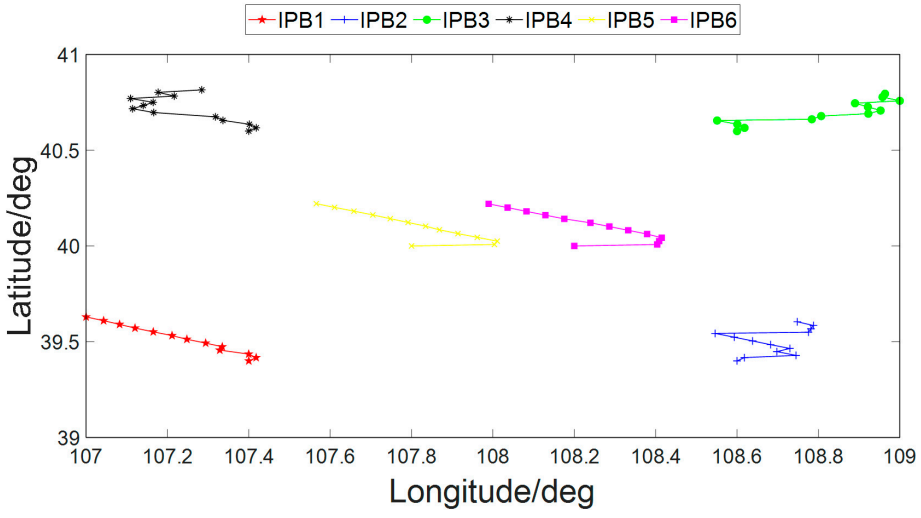

(**a**)

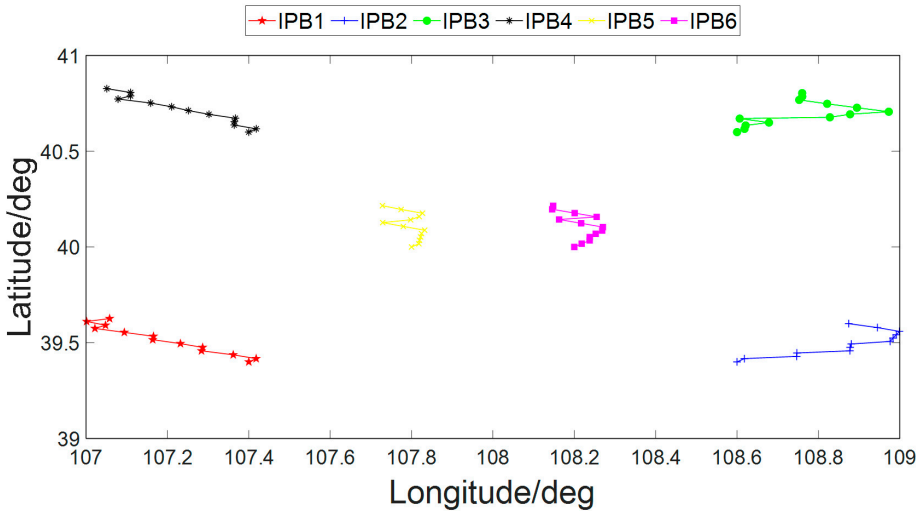

(**b**)

Figure 10. *Cont.*

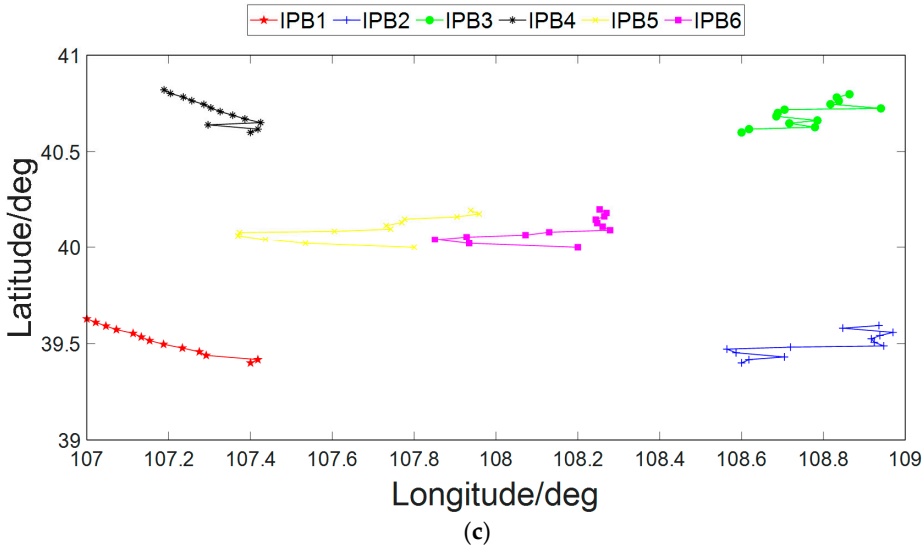

(**c**)

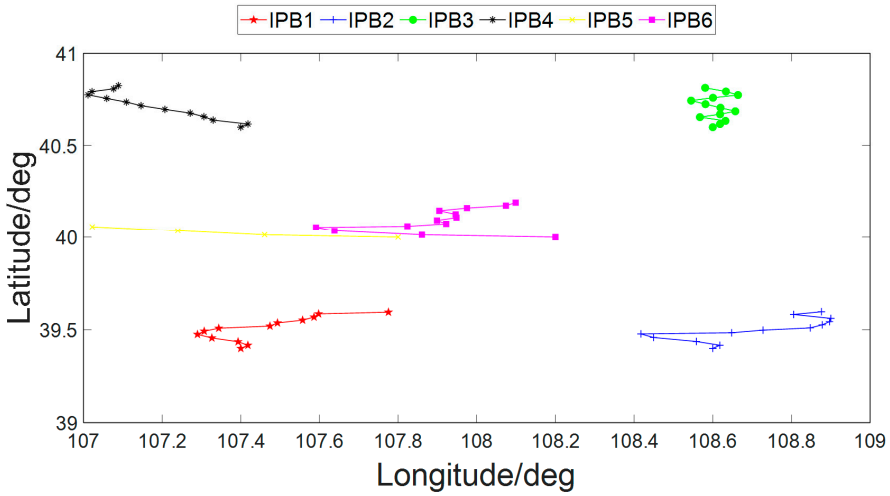

(**d**)

Figure 10. Horizontal trajectory comparison for IPCBs with different initial flight altitudes: (**a**) IPB5 and IPB6 at 20 km initially; (**b**) IPB5 and IPB6 at 21 km initially; (**c**) IPB5 and IPB6 at 23 km initially; (**d**) IPB5 and IPB6 at 24 km initially. (Horizontal trajectory for IPCB with IPB5 and IPB6 at 22 km initially, please refer to Figure 7).

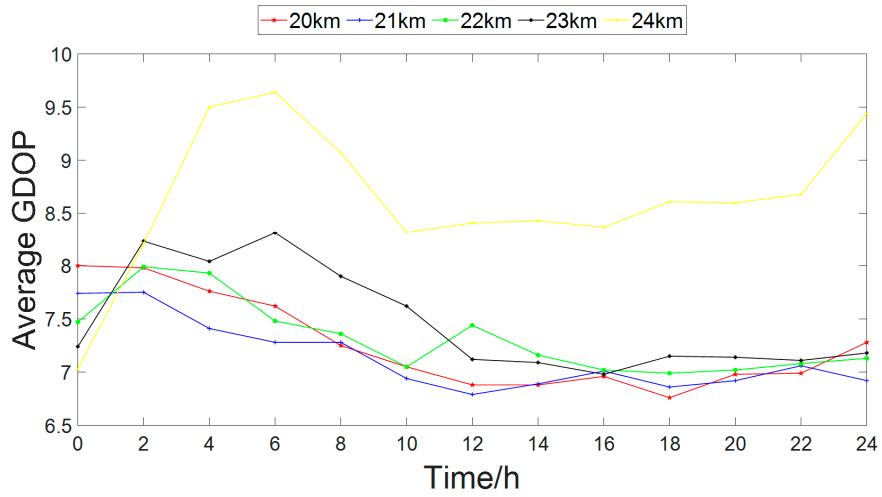

Figure 11. GDOP comparison for IPCBs with different initial flight altitudes.

7.4. Discussion about IPCBs with Different Initial Horizontal Layouts

The initial horizontal layout of an IPCB also has a significant impact on its geometry performance. This section adjusts the initial latitude of IPB5 and IPB6 from south to north, as illustrated in Figure 12, while other conditions remain untouched. The planning results are compared in Figures 13–15.

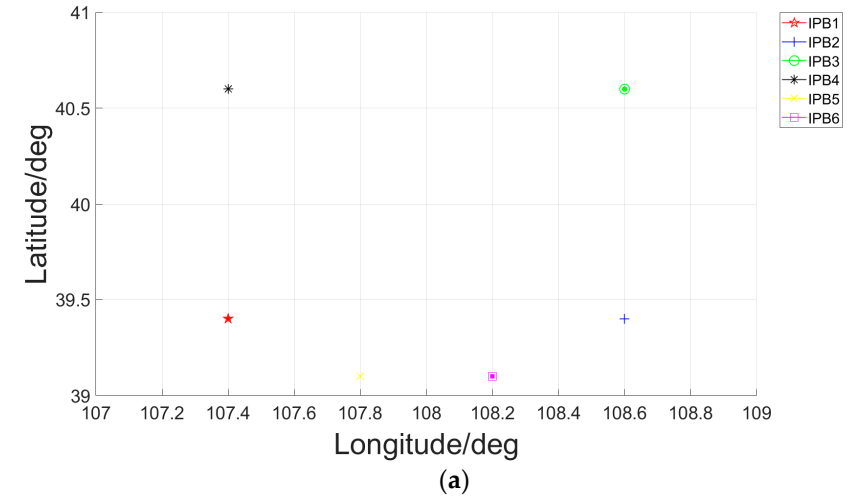

(**a**)

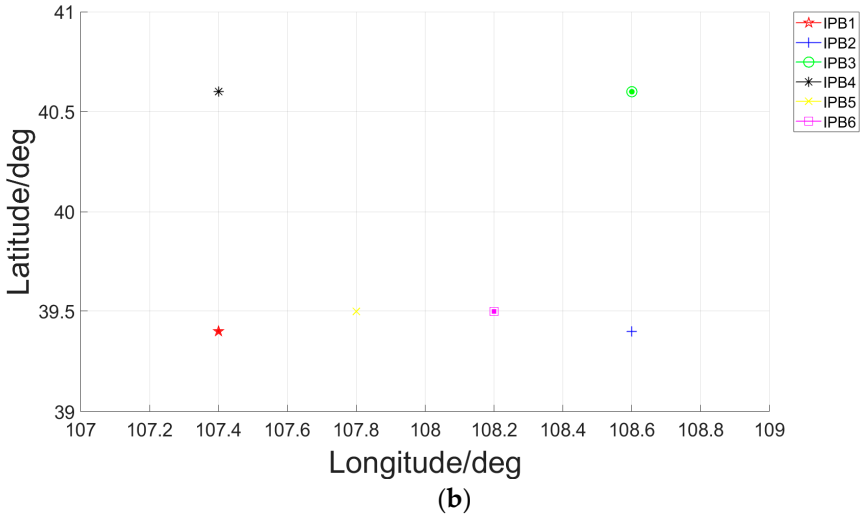

(**b**)

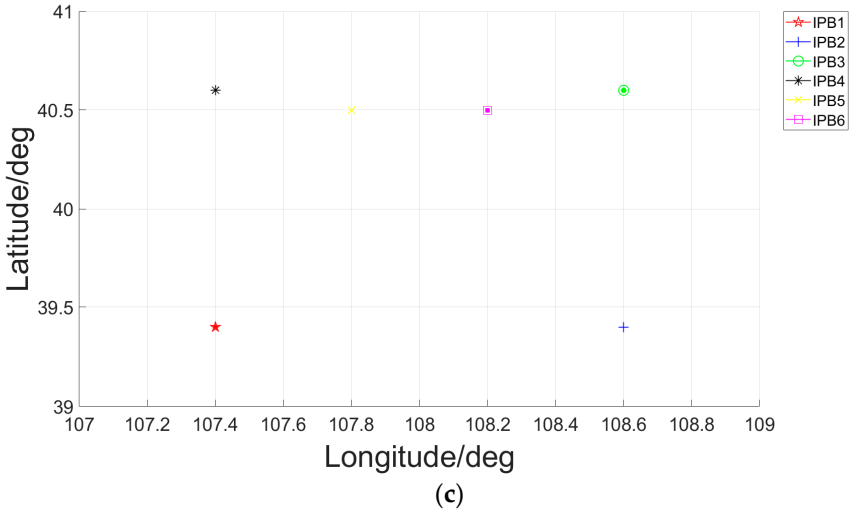

(**c**)

Figure 12. *Cont.*

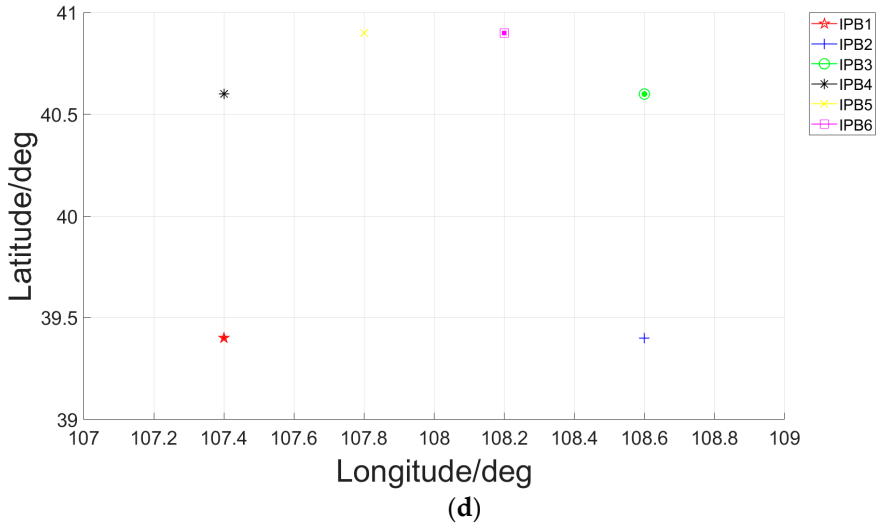

(**d**)

Figure 12. Illustration of different initial horizontal layouts: (**a**) Layout 1 (IPB5 and IPB6 at 39.1° N); (**b**) Layout 2 (IPB5 and IPB6 at 39.5° N); (**c**) Layout 4 (IPB5 and IPB6 at 40.5° N); (**d**) Layout 5 (IPB5 and IPB6 at 40.9° N). (Layout 3 (IPB5 and IPB6 at 40° N), please refered to Figure 5a).

Figures 13–15 and Table 4 show that IPCB can obtain better performance in deploying IPBs with high altitudes to positions near the airspace center (layout 3) than to positions near airspace borders (Layout 1 and Layout 5).

Table 4. Simulation results of IPCBs with different initial horizontal layouts.

Initial Horizontal Layout	Average GDOP
Layout 1	10.88
Layout 2	9.53
Layout 3	7.32
Layout 4	10.83
Layout 5	22.14

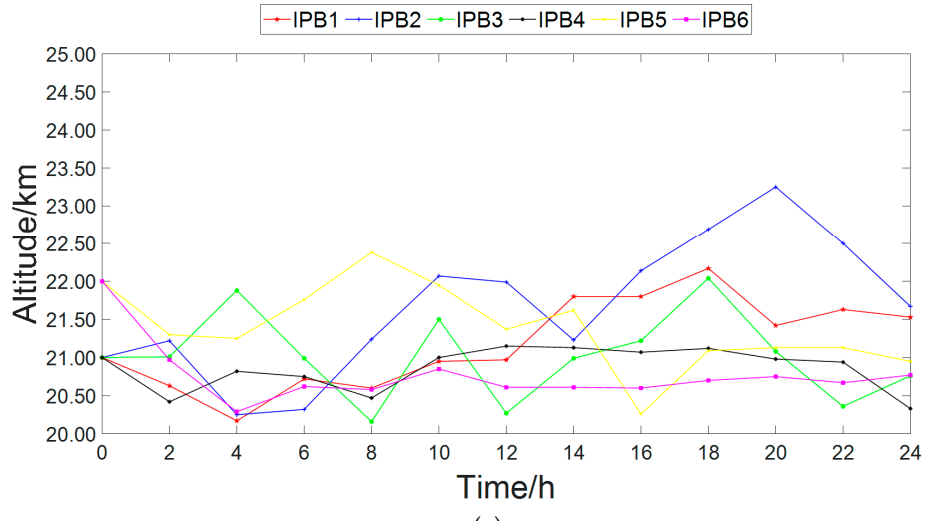

(**a**)

Figure 13. *Cont.*

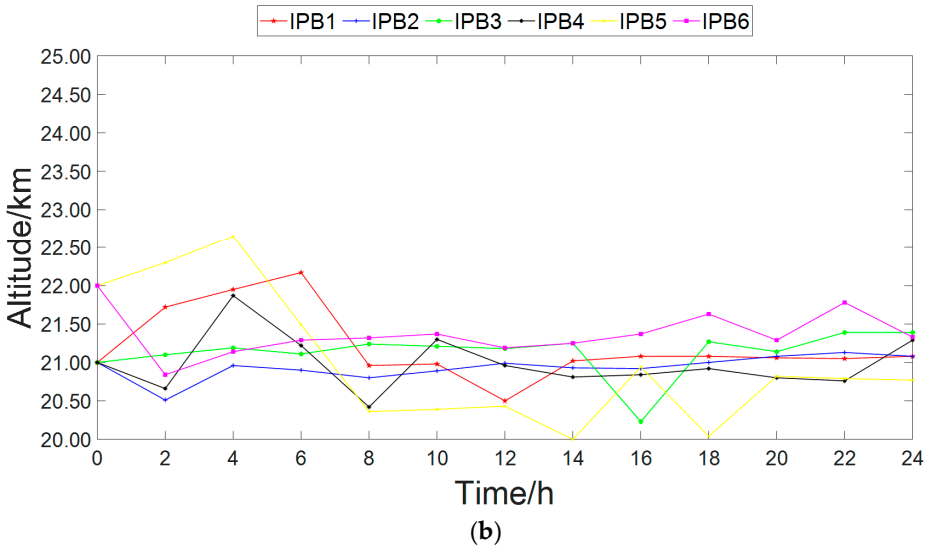

(**b**)

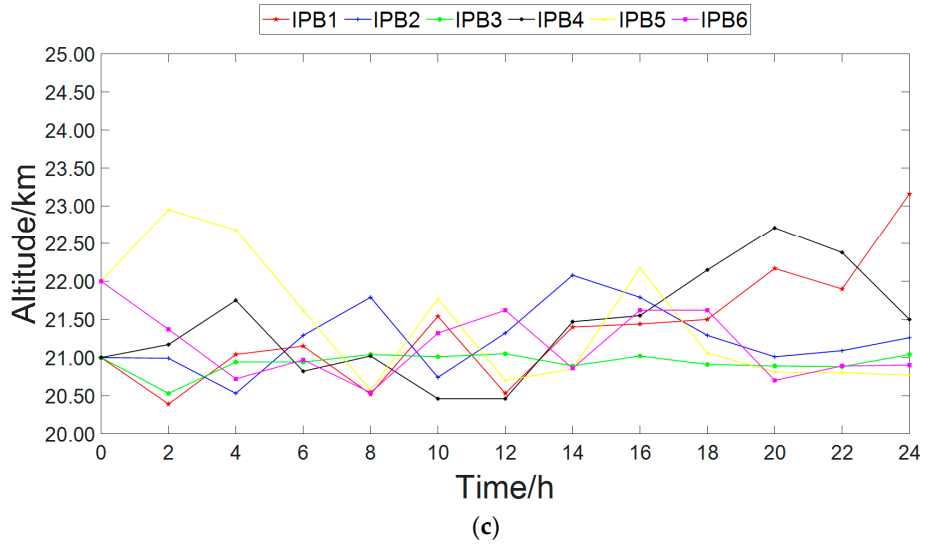

(**c**)

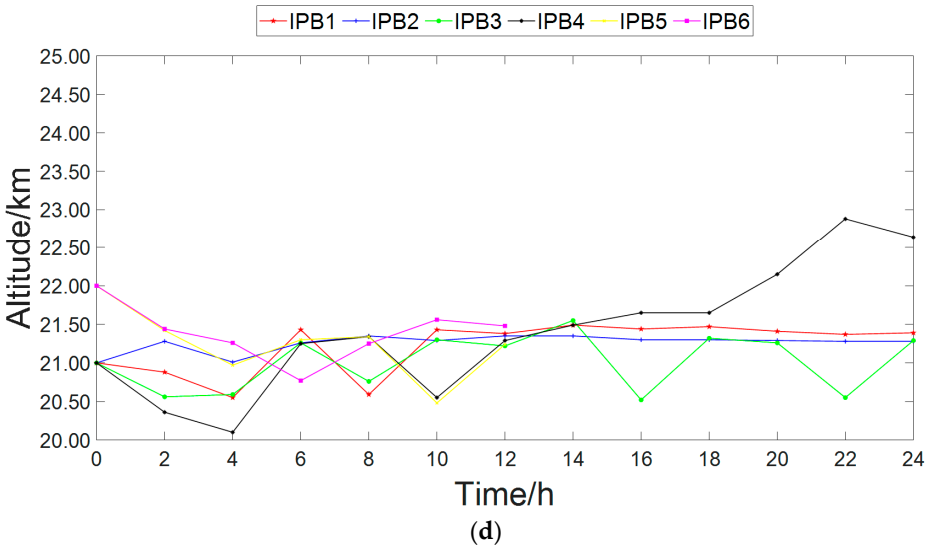

(**d**)

Figure 13. Flight altitude comparison for IPCBs with different initial horizontal layouts: (**a**) Layout 1; (**b**) Layout 2; (**c**) Layout 4; (**d**) Layout 5. (Flight altitude for IPCB with initial Layout 3, please refer to Figure 6).

Furthermore, Figure 15 shows that IPCBs with Layout 1 and Layout 5 have approximate initial GDOPs. However, their performance displays a different tendency as time goes on. A similar case occurs in IPCBs with Layout 2 and Layout 4. Data in Table 5 also shows that Layout 1 performs better than Layout 5, and Layout 2 performs better than Layout 4. These phenomena may be derived from the winds used in the simulations. In the feasible flight altitude range (21~24 km), the meridional winds are all southerly, leading to all the IPBs moving northward. So, IPCBs with low initial latitudes perform better than IPCBs with high initial latitudes. It is especially obvious in Layout 5, in which IPB5 and IPB6 fly out of the approved airspace quickly due to the short distance between their initial positions and the north border of the airspace.

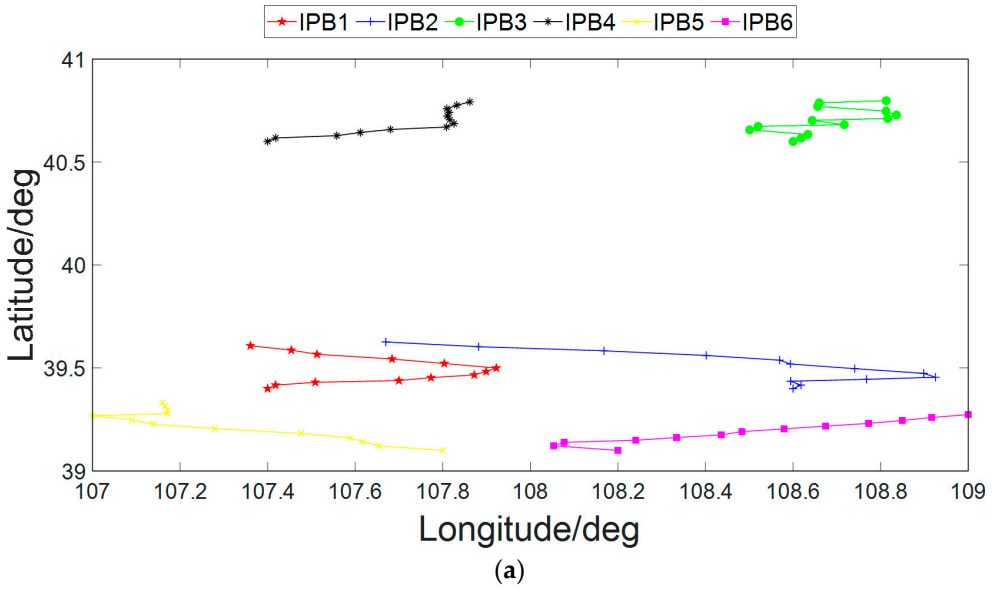

(**a**)

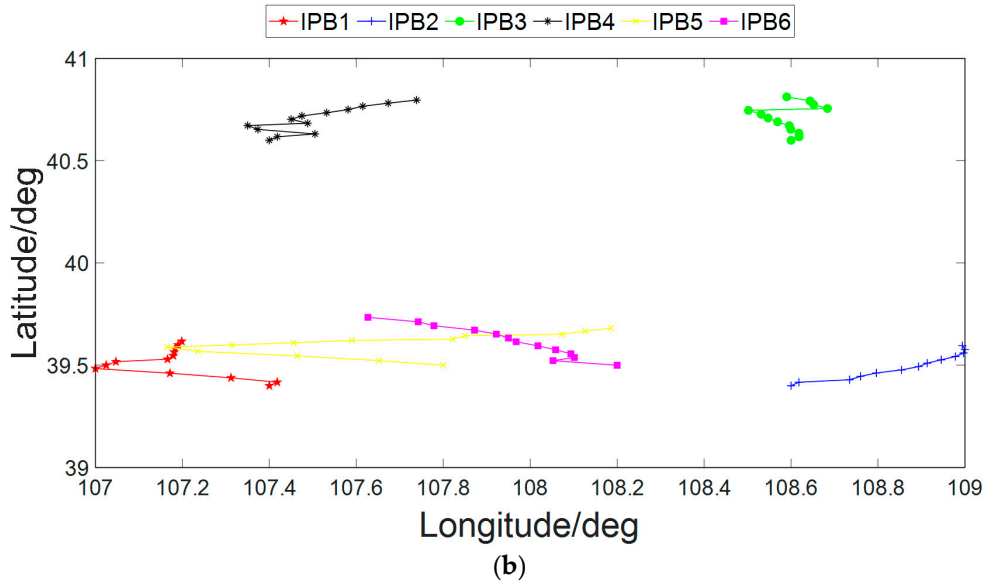

(**b**)

Figure 14. *Cont.*

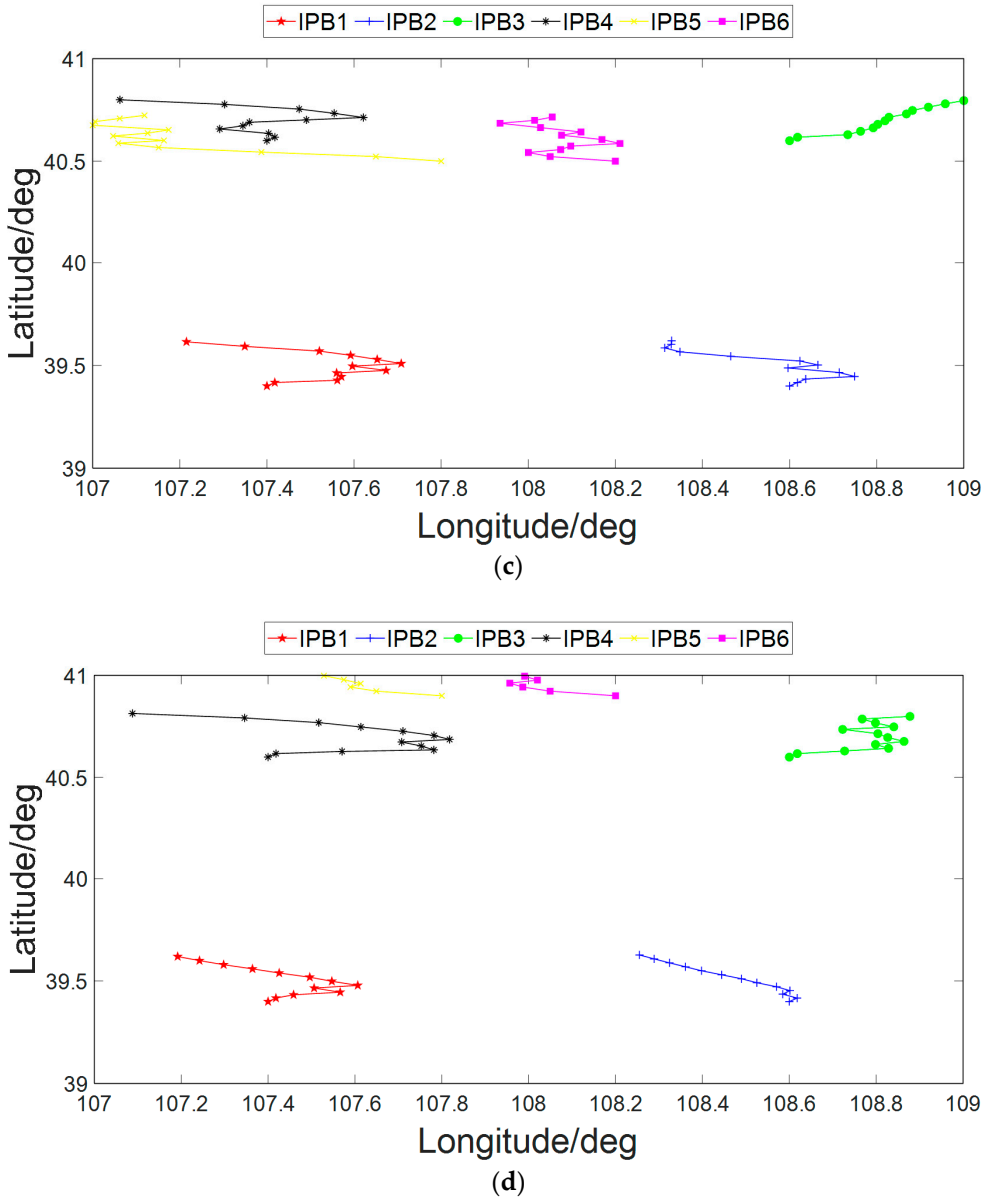

Figure 14. Horizontal trajectory comparison for IPCBs with different initial horizontal layouts: (**a**) Layout 1; (**b**) Layout 2; (**c**) Layout 4; (**d**) Layout 5. (Horizontal trajectory for IPCB with initial Layout 3, please refer to Figure 7).

In winds with quasi-zero wind layers, the direction reversion rule of zonal wind can be employed to improve IPCB geometry configuration. In contrast, no proper rule of meridional wind can be employed. To achieve good performance throughout the whole service duration, the wind is suggested to be treated as a notable factor in the initial horizontal layout design of IPCB.

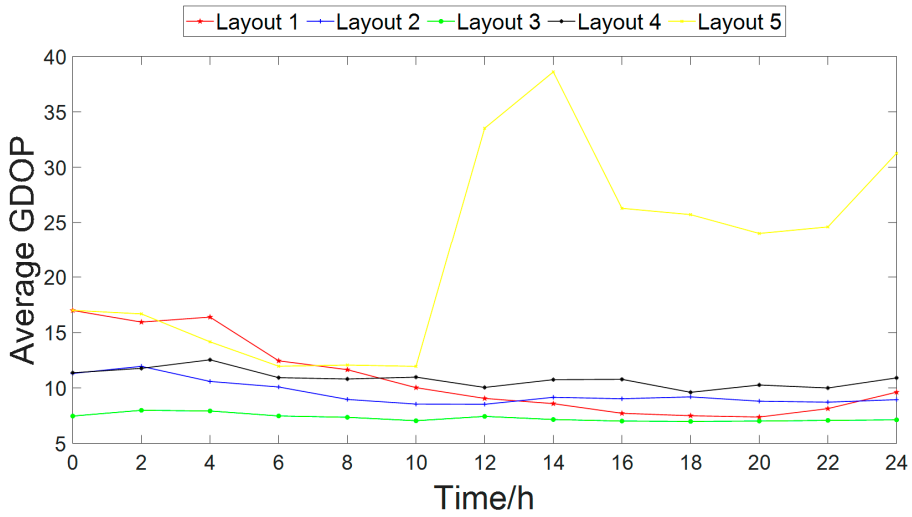

Figure 15. GDOP comparison for IPCBs with different initial horizontal layouts.

Table 5. Coefficients used to fit wind without quasi-zero wind layer.

Symbol	Physical Meaning	Value
c_m	meridional wind coefficients	−0.5066, 4.3171, −14.6477, 27.7923, −36.4969, 32.8921, −13.9287, −0.2023
c_z	zonal wind coefficients	−40.2337, 321.8428, −1018.3275, 1597.1910, −1263.8719, 461.2160, −94.6881, 40.2845

7.5. Discussion about IPCBs in Winds with/without Quasi-Zero Wind Layer

From previous discussions, it can be seen that the quasi-zero wind layer plays an important role in IPCB geometry configuration. However, the quasi-zero wind layer does not always exist. In this section, wind without a quasi-zero wind layer is used to implement the planning. The wind coefficients used in this section are listed in Table 5. The comparison of wind in this section and wind in Section 7.2 is illustrated in Figure 16. The planning result is shown in Figures 17–19.

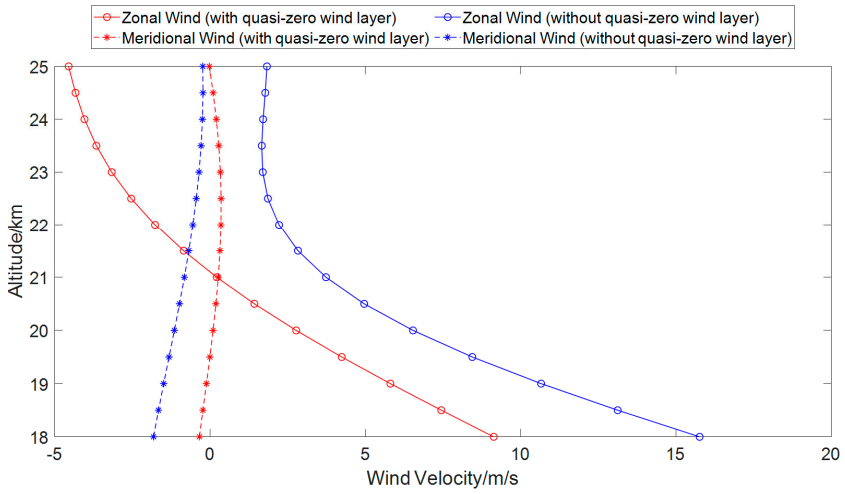

Figure 16. Wind comparison (with/without quasi-zero wind layer).

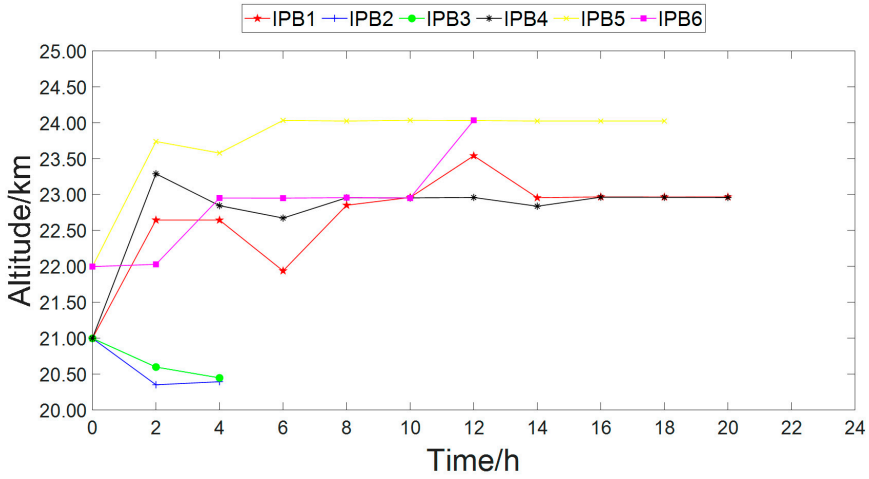

Figure 17. Flight altitude of the IPCB in the wind without a quasi-zero wind layer.

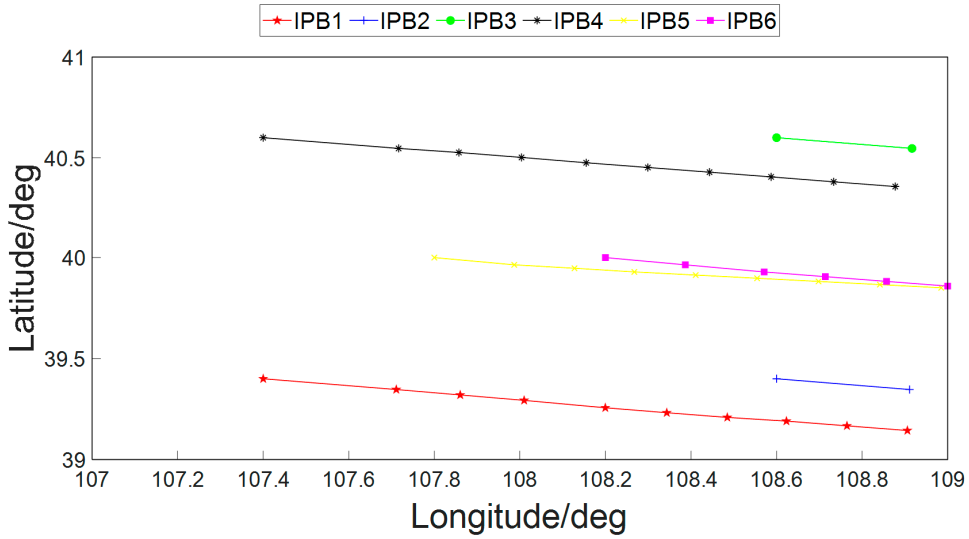

Figure 18. Flight trajectory of the IPCB in the wind without a quasi-zero wind layer.

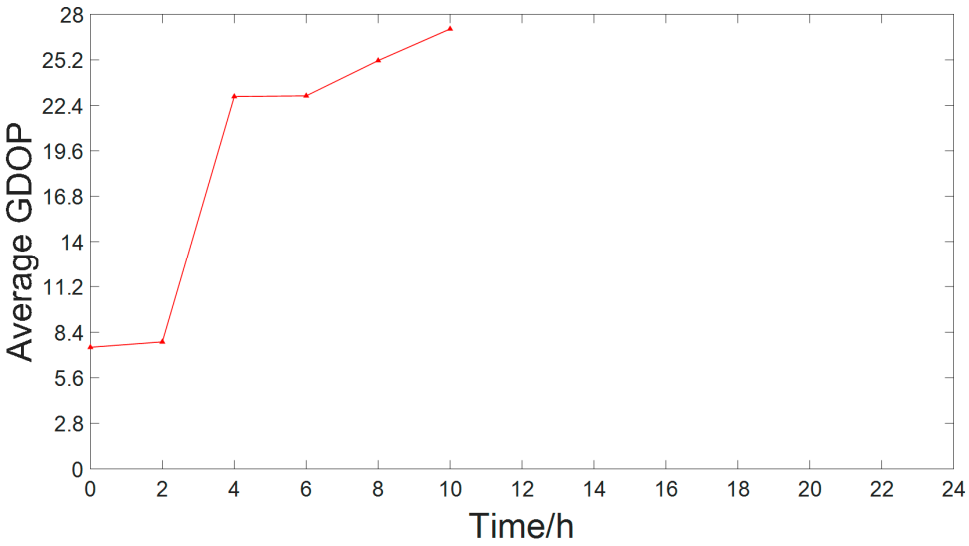

Figure 19. GDOP comparison for IPCBs in winds with/without quasi-zero wind layers.

From Figures 17–19, it can be seen that in winds without a quasi-zero wind layer, zonal trajectory direction reversion does not occur since wind direction reversion does not occur. In addition, the wind velocity is bigger than the wind velocity in Section 7.2, so some IPBs fly out of the approved airspace in a short time, such as IPB2 and IPB3 in Figure 18. This leads to a decrease in the number of available IPBs in the IPCB and deterioration in the IPCB geometry configuration. In order to lengthen IPBs' flight time in the approved airspace, the planning algorithm tends to adjust IPBs' flight altitude to 23~24 km, where wind velocity is small, as IPB1, IPB 4, IPB 5, and IPB6 in Figure 17 illustrate.

By comparing planning results in this section with results in Section 7.2, it can be seen that the results in winds with quasi-zero wind layers are significantly better than those in winds without quasi-zero wind layers. It indicates the significance of the quasi-zero wind layer in improving IPCB geometry performance.

To improve IPCB performance in winds without quasi-zero wind layers, measures such as altering the initial layout, increasing the initial number of IPBs, or supplementing IPBs dynamically can be taken.

Since IPCB achieves its flight mainly by buoyancy and winds, it is sensitive to its running environment. Environment fluctuations or different environment models may bring different results, which can be analyzed in detail in the future.

7.6. Discussion about Uncertain Environment

The simulations above are based on the assumption of a deterministic environment in which wind velocities and atmospheric density are steady. However, uncertain and unknown factors exist in the IPCB running environment.

Conway has investigated horizontal velocity in the midlatitude stratosphere using the observation data of Project Loon and has found the existence of horizontal wind velocity perturbations [61]. Wolf has proposed a model for modeling uncertain winds, which employed a Von Mises distribution to simulate the direction of uncertain wind and a Gaussian distribution to simulate the magnitude of uncertain wind [39]. However, in general, direct observations of winds in the stratosphere are sparse, so a precise model of stratospheric wind is very challenging.

Since this paper focuses on the problem of IPCB geometry configuration, we will not discuss the environment model in detail.

An uncertain environment may degrade the effect of the proposed algorithm because the uncertainty may make IPBs' trajectories deviate from expectation, and as a result, the geometry configuration of IPCB cannot reach the ideal state.

To improve robustness, data filters or environment prediction models can be developed. When perceiving uncertain factors, data filters and prediction models can help to filter out data errors and keep real environment changes. The IPCB can update the environment model and implement the planning algorithm with the new environment model.

8. Conclusions

IPCBs are a novel pseudolite application with many advantages and unique features. Compared with traditional ground-based pseudolites and other air-based pseudolites, IPCB uses high-altitude balloons to achieve higher altitudes and wider coverage. Compared with pseudolites based on powered platforms, IPCBs can save energy costs greatly by utilizing buoyancy and wind. When bringing advantages to applications, these features also bring great challenges to IPCB geometry configuration.

This paper proposes an IPCB geometry configuration planning algorithm that considers the unique features of the IPCB and implements simulations to verify the effectiveness of the proposed algorithm. Furthermore, this paper implements simulations with some typical IPCB geometry configurations and compares their performances.

Simulations show that, in the vertical direction, it can achieve better performance to deploy IPCBs at the altitude of the local quasi-zero wind layer; if the expected service duration is short, IPCBs can be deployed at higher altitudes, and if the expected service

duration is long, IPCBs can be deployed at the altitude of local quasi-zero wind layer. In the horizontal direction, the direction of local wind should be treated as an important factor in designing the initial constellation geometry configuration. A quasi-zero wind layer is helpful in improving IPCB geometry performance.

In the future, attention can be paid to approaches to enhance robust algorithms and enhance tolerance to different environment models. Improvements in algorithm performance are also desired to realize real-time control.

Author Contributions: Conceptualization, Y.Q.; methodology, Y.Q. and S.W.; software, Y.Q.; validation, T.P. and H.F.; writing—original draft preparation, Y.Q.; writing—review and editing, S.W. and T.P.; visualization, Y.Q. and T.P.; supervision, S.W. All authors have read and agreed to the published version of the manuscript.

Funding: This work was funded by the National Key Research and Development Program of China (Grant No. 2022YFB3901805).

Data Availability Statement: Data are contained within the article.

Conflicts of Interest: The authors declare no conflicts of interest.

References

1. Klein, D.; Parkinson, B.W. The use of pseudo-satellites for improving GPS performance. *Navig. J. Inst. Navig.* **1984**, *31*, 303–315. [CrossRef]
2. Morley, T.; Lachapelle, G. GPS augmentation with pseudolites for navigation in constricted waterways. *Navig. J. Inst. Navig.* **1997**, *44*, 359–372. [CrossRef]
3. Wang, J. Pseudolite applications in positioning and navigation: Progress and problems. *J. Glob. Position. Syst.* **2002**, *1*, 48–56. [CrossRef]
4. Dixon, C.S.; Morrison, R.G. A pseudolite-based maritime navigation system: Concept through to demonstration. *J. Glob. Position. Syst.* **2008**, *7*, 9–17. [CrossRef]
5. Ma, C.; Yang, J.; Chen, J. Satellite-Ground Joint Positioning System Based on Pseudolite. In Proceedings of the 2018 IEEE CSAA Guidance, Navigation and Control Conference, CGNCC, Xiamen, China, 10–12 August 2018. [CrossRef]
6. Sheng, C.; Gan, X.; Yu, B.; Zhang, J. Precise point positioning algorithm for pseudolite combined with GNSS in a constrained observation environment. *Sensors* **2020**, *20*, 1120. [CrossRef]
7. Liu, T.; Liu, J.; Wang, J.; Zhang, H.; Zhang, B.; Ma, Y.; Sun, M.; Lv, Z.; Xu, G. Pseudolites to support location services in smart cities: Review and prospects. *Smart Cities* **2023**, *6*, 2081–2105. [CrossRef]
8. Kayhan, Ö.; Yücel, Ö.; Hastaoğlu, M.A. Simulation and control of serviceable stratospheric balloons traversing a region via transport phenomena and PID. *Aerosp. Sci. Technol.* **2016**, *53*, 232–240. [CrossRef]
9. Jiang, Y.; Lv, M.; Zhu, W.; Du, H.; Zhang, L.; Li, J. A method of 3-D region controlling for scientific balloon long-endurance flight in the real wind. *Aerosp. Sci. Technol.* **2020**, *97*, 1–11. [CrossRef]
10. Zhu, W.; Xu, Y.; Du, H.; Li, J. Thermal performance of high-altitude solar powered scientific balloon. *Renew. Energy* **2019**, *135*, 1078–1096. [CrossRef]
11. Jiang, Y.; Lv, M.; Qu, Z.; Zhang, L. Performance evaluation for scientific balloon station-keeping strategies considering energy management strategy. *Renew. Energy* **2020**, *156*, 290–302. [CrossRef]
12. Li, C.; Luo, R.; Chen, T. New idea for stratospheric communications—Google Loon. *Commun. Technol.* **2015**, *48*, 125–129. [CrossRef]
13. Deng, X.; Yang, X.; Zhu, B.; Ma, Z.; Hou, Z. Simulation research and key technologies analysis of intelligent stratospheric aerostat Loon. *Acta Aeronaut. Et Astronaut. Sin.* **2023**, *44*, 127412. [CrossRef]
14. Rabinowitz, M.; Parkinson, B.W.; Cohen, C.E.; O'Connor, M.L.; Lawrence, D.G. A system using LEO telecommunication satellites for rapid acquisition of integer cycle ambiguities. In Proceedings of the Position Location and Navigation Symposium, Palm Springs, CA, USA, 20–23 April 1996; pp. 137–145. [CrossRef]
15. Li, X.; Li, X.; Ma, F.; Yuan, Y.; Zhang, K.; Zhou, F.; Zhang, X. Improved PPP ambiguity resolution with the assistance of multiple LEO constellations and signals. *Remote Sens.* **2019**, *11*, 408. [CrossRef]
16. Ge, H.; Li, B.; Jia, S.; Nie, Y.; Wu, T.; Yang, Z.; Shang, J.; Zheng, Y.; Ge, M. LEO enhanced global navigation satellite system (LeGNSS): Progress, opportunities, and challenges. *Geo-Spat. Inf. Sci.* **2022**, *25*, 1–13. [CrossRef]
17. Yuan, H.; Chen, X.; Luo, R.; Wan, H.; Zhang, Y.; Li, R.; Yang, G. Review of the development trend of LEO-based navigation system. *Navig. Position. Timing* **2022**, *9*, 1–11. [CrossRef]
18. Zhang, Y.; Fan, L.; Liu, J.; Li, Z. Feasibility analysis of commercial broadband LEO constellation incorporated into the national comprehensive PNT system. *Navig. Position. Timing* **2022**, *10*, 26–36. [CrossRef]

19. Dai, L.; Wang, J.; Tsujii, T.; Rizos, C. Pseudolite Applications in Positioning and Navigation: Modelling and Geometric Analysis. In Proceedings of the International Symposium on Kinematic Systems in Geodesy, Geomatics & Navigation (KIS2001), Banff, AB, Canada, 5–8 June 2001.
20. Chandu, B.; Pant, R.S.; Moudgalya, K. Modeling and Simulation of a Precision Navigation System Using Pseudolites Mounted on Airships. In Proceedings of the 7th AIAA Aviation Technology, Integration and Operations Conference, Belfast, Northern Ireland, 18–20 September 2007.
21. Oktay, H. Airborne pseudolites in a global positioning system degraded environment. In Proceedings of the 5th International Conference on Recent Advances in Space Technologies–RAST2011, Istanbul, Turkey, 9–11 June 2011. [CrossRef]
22. Tsujii, T.; Harigae, M.; Barnes, J.; Wang, J.; Rizos, C. Experiments of inverted pseudolite positioning for airship-based GPS augmentation system. In Proceedings of the 15th International Technical Meeting of the Satellite Division of the U.S. Institute of Navigation, Portland, OR, USA, 24–27 September 2002; pp. 1689–1695.
23. Sultana, Q.; Sunehra, D.; Ratnam, D.V.; Rao, P.S.; Sarma, A.D. Significance of instrumental biases and dilution of precision in the context of GAGAN. *Indian J. Radio Space Phys.* **2007**, *36*, 405–410.
24. Quddusa, S.; Dhiraj, S.; Vemuri, S.S.; Achanta, D.S. Effects of pseudolite positioning on DOP in LAAS. *Positioning* **2010**, *1*, 18–26. [CrossRef]
25. Wang, J.; Li, H.; Lu, J.; Li, K.; Li, H.; Yang, L.; Li, Y. A PSO-Based Layout Method for GNSS Pseudolite System. In Proceedings of the ICIT 2017, Singapore, 27–29 December 2017. [CrossRef]
26. Jiang, M.; Li, R.; Liu, W. Research on geometric configuration of pseudolite positioning system. *Comput. Eng. Appl.* **2017**, *53*, 271–276.
27. Tang, W.; Chen, J.; Yu, C.; Ding, J.; Wang, R. A new ground-based pseudolite system deployment algorithm based on MOPSO. *Sensors* **2021**, *21*, 5364. [CrossRef]
28. Du, H.; Lv, M.; Li, J.; Zhu, W.; Zhang, L.; Wu, Y. Station-keeping performance analysis for high altitude balloon with altitude control system. *Aerosp. Sci. Technol.* **2019**, *92*, 644–652. [CrossRef]
29. Du, H.; Li, J.; Zhu, W.; Qu, Z.; Zhang, L.; Lv, M. Flight performance simulation and station-keeping endurance analysis for stratospheric super-pressure balloon in real wind field. *Aerosp. Sci. Technol.* **2019**, *86*, 1–10. [CrossRef]
30. Du, H.; Lv, M.; Zhang, L.; Zhu, W.; Wu, Y.; Li, J. Energy management strategy design and station-keeping strategy optimization for high altitude balloon with altitude control system. *Aerosp. Sci. Technol.* **2019**, *93*, 1–9. [CrossRef]
31. Song, J.; Hou, C.; Xue, G.; Ma, M. Study of constellation design of pseudolites based on improved adaptive genetic algorithm. *J. Commun.* **2016**, *11*, 879–885. [CrossRef]
32. Tian, R.; Cui, Z.; Zhang, S.; Wang, D. Overview of navigation augmentation technology based on LEO. *Navig. Position. Timing* **2021**, *8*, 66–81. [CrossRef]
33. Kaplan, E.D.; Hegarty, C.J. *Understanding GPS: Principles and Applications, 2nd ed*; Artech House Inc.: Norword, MA, USA, 2006; p. 02062.
34. Teng, Y.; Wang, J.; Huang, Q. Mathematical minimum of geometric dilution of precision (GDOP) for dual-GNSS constellations. *Adv. Space Res.* **2016**, *57*, 183–188. [CrossRef]
35. Nalineekumari, A.; Sasibhushana, R.G.; Ashok, K.N. GDOP analysis with optimal satellite using GA for southern region of Indian subcontinent. *Procedia Comput. Sci.* **2018**, *143*, 303–308. [CrossRef]
36. Teng, Y.; Wang, J. A closed-form formula to calculate geometric dilution of precision (GDOP) for multi-GNSS constellations. *GPS Solut.* **2016**, *20*, 331–339. [CrossRef]
37. Li, D.; Deng, P.; Liu, B.; Qu, Y.; Zeng, L.; Liu, T. Research on the Dynamic Configuration of Air-Based Pseudolite Network. In *China Satellite Navigation Conference (CSNC) 2015 Proceedings*; Springer: Berlin/Heidelberg, Germany, 2015; Volume II, pp. 357–367.
38. Blackmore, B.; Kuwata, Y.; Wolf, M.T.; Assad, C.; Fathpour, N.; Newman, C.; Elfes, A. Global Reachability and Path Planning for Planetary Exploration with Montgolfirer Balloons. In Proceedings of the 2010 IEEE International Conference on Robotics and Automation, Anchorage Convention District, Anchorage, AK, USA, 3–8 May 2010.
39. Wolf, M.T.; Blackmore, L.; Kuwata, Y.; Fathpour, N.; Newman, C. Probabilistic Motion Planning of Balloons in Strong, Uncertain Wind Fields. In Proceedings of the IEEE International Conference on Robotics & Automation, Anchorage, AK, USA, 3–7 May 2010. [CrossRef]
40. Zhai, J.; Yang, X.; Deng, X.; Long, Y.; Zhang, J.; Bai, F. Global path planning of stratospheric aerostat in uncertain wind field. *J. Beijing Univ. Aeronaut. Astronaut.* **2023**, *49*, 1116–1126. [CrossRef]
41. Bellemare, M.G.; Candido, S.; Castro, P.S.; Gong, J.; Machado, M.C.; Moitra, S.; Ponda, S.S.; Wang, Z. Autonomous navigation of stratospheric balloons using reinforcement learning. *Nature* **2020**, *588*, 77–82. [CrossRef]
42. Furfaro, R.; Lunine, J.I.; Elfes, A.; Reh, K. Wind-based navigation of a hot-air balloon on Titan: A feasible study. In Proceedings of the SPIE Defense and Security Symposium, Orlando, FL, USA, 18–20 March 2008. [CrossRef]
43. Hedin, A.E.; Biondi, M.A.; Burnside, R.G.; Hernandez, G.; Johnson, R.M.; Killeen, T.L.; Mazaudier, C.; Meriwether, J.W.; Salah, J.E.; Sica, R.J.; et al. Revised global model of thermosphere winds using satellite and ground-based observations. *J. Geophys. Res.* **1991**, *96*, 7657–7688. [CrossRef]
44. Mueller, J.B.; Zhao, Y.J.; Garrard, W.L. Optimal ascent trajectories for stratospheric airships using wind energy. *J. Guid. Control. Dyn.* **2009**, *32*, 1232–1245. [CrossRef]

45. Lee, S.; Bang, H. Three-dimensional ascent trajectory optimization for stratospheric airship platforms in the jet stream. *J. Guid. Control. Dyn.* **2007**, *30*, 1341–1352. [CrossRef]
46. Sun, S.; Li, Z.; Tian, K. Modeling and trajectory planning of return process for a class of airship with wind field. *Aerosp. Control. Appl.* **2014**, *40*, 37–41. [CrossRef]
47. Zhang, X.; Chen, L.; Quan, T. Study of ascent trajectory for stratospheric airship in the jet stream. *Electron. Des. Eng.* **2014**, *22*, 11–13.
48. Belmont, A.D.; Dartt, D.G.; Nastrom, G.D. Variations of stratospheric zonal winds, 20–65 km, 1961–1971. *J. Appl. Meteorol.* **1975**, *14*, 585–594. [CrossRef]
49. Tao, M.; He, J.; Liu, Y. Analysis of the characteristics of the stratospheric quasi-zero wind layer and the effects of the quasi-biennial oscillation on it. *Clim. Environ. Res.* **2012**, *17*, 92–102. [CrossRef]
50. Chang, X.; Bai, Y.; Fu, W.; Yan, J. Research on fixed-point aerostat based on its special stratosphere wind field. *J. Northwestern Polytech. Univ.* **2014**, *32*, 12–17.
51. Deng, X.; Li, K.; Yu, C.; Yang, X.; Hou, Z. Station-keeping performance of novel near-space aerostat in quasi-zero wind layer. *J. Natl. Univ. Def. Technol.* **2019**, *41*, 5–12. [CrossRef]
52. Chen, B.; Liu, Y.; Liu, L.; Shen, X.; Zhang, Y. Characteristics of spatial–temporal distribution of the stratospheric quasi-zero wind layer in low-latitude regions. *Clim. Environ. Res.* **2018**, *23*, 657–669. [CrossRef]
53. Roney, J.A. Statistical wind analysis for near-space applications. *J. Atmos. Sol. Terr. Phys.* **2007**, *69*, 1485–1501. [CrossRef]
54. Mirjalili, S.; Lewis, A. The whale optimization algorithm. *Adv. Eng. Softw.* **2016**, *95*, 51–67. [CrossRef]
55. Mafarja, M.M.; Mirjalili, S. Hybrid whale optimization algorithm with simulated annealing for feature selection. *Neurocomputing* **2017**, *260*, 302–312. [CrossRef]
56. Xiong, G.; Zhang, J.; Shi, D.; He, Y. Parameter extraction of solar photovoltaic models using an improved whale optimization algorithm. *Energy Convers. Manag.* **2018**, *174*, 388–405. [CrossRef]
57. Ling, Y.; Zhou, Y.; Luo, Q. Lévy flight trajectory-based whale optimization algorithm for global optimization. *IEEE Access* **2017**, *5*, 6168–6186. [CrossRef]
58. Yan, Z.; Wang, S.; Liu, B.; Li, X. Application of Whale Optimization Algorithm in Optimal Allocation of Water Resources. In Proceedings of the 2018 3rd International Conference on Advances in Energy and Environment Research (ICAEER 2018), Guilin, China, 10–12 August 2018. [CrossRef]
59. Kennedy, J.; Eberhart, R. Particle Swarm Optimization. In Proceedings of the ICNN95–International Conference on Neural Networks, Perth, WA, Australia, 27 November–1 December 1995. [CrossRef]
60. Neri, R.; Tirronen, V. Scale factor local search in differential evolution. *Memetic Comp.* **2009**, *1*, 153–171. [CrossRef]
61. Conway, J.P.; Bodeker, G.E.; Waugh, D.W.; Murphy, D.J.; Cameron, C.; Lewis, J. Using project Loon superpressure balloon observations to investigate the inertial peak in the intrinsic wind spectrum in the midlattitude stratosphere. *J. Geophys. Res. Atmos.* **2019**, *124*, 8594–8604. [CrossRef]